Scanning Microscopy

Volume 10 | Number 1 Article 2

12-6-1995

Spatial Dependence of Electron-Hole Pair Creation in Ion-Solid and Electron-Solid Interactions

F. J. García de Abajo
Universidad del Pais Vasco/EHU, ccpgaabf@si.ehu.es

Scanning Microscopy, Vol. 10, No. 1, 1996 (Pages 9-32) 0891-7035/96$5.00+.25
Scanning Microscopy International, Chicago (AMF O'Hare), IL 60666 USA

SPATIAL DEPENDENCE OF ELECTRON-HOLE PAIR CREATION IN ION-SOLID AND ELECTRON-SOLID INTERACTIONS

F.J. García de Abajo

Depto. de CCIA, Facultad de Informática, Universidad del País Vasco/EHU,
Aptdo. 649, 20080 San Sebastián, Spain
Telephone number: 34-43-218000 / FAX number: 34-43-212236 / E.mail: ccpgaabf@si.ehu.es

(Received for publication May 8, 1995 and in revised form December 6, 1995)

Abstract

The problem of electron excitation induced by interaction of charged particles with solids is investigated on theoretical grounds. The excitation probability is calculated both in homogeneous media and at surfaces. The surface wake potential, needed in the latter, is reviewed. The cases of transmission and aloof geometries are considered separately. Surface plasmons are shown to play a crucial role in the latter. An application to coincidence scanning transmission electron microscopy (STEM) experiments is also discussed. Finally, a spatial representation of the excitation probability is presented.

Key Words: Electron emission, wake potential, surfaces, plasmons.

Introduction

Electron emission induced in condensed matter by fast charged particles has been the subject of many experimental and theoretical studies since its discovery early this century [67, 72]. A realistic theoretical description of the phenomenon needs to incorporate both electron excitation and transport. The latter consists of a complicated cascade of successive electron scattering processes and the eventual crossing of the surface. Starting several decades ago, with the first plausible descriptions of electron emission [2, 5, 70, 75], the electron transport has been analyzed by different authors applying Monte Carlo simulation techniques [10], solving the appropriate Boltzmann equation [10, 65], or using semi-classical approximations [69]. A reasonable agreement with experiments has been achieved [28]. However, there are some problems connected with particle-induced electron emission that still lack a first-principles description. For instance, that is the case in the transport of electrons near surfaces and in the role of surface plasmons in electron emission. Also, the basic theory of the so-called shock-electrons [6, 66], which are thought to travel perpendicularly to the shock front of the wake of electron density fluctuations induced by a charge moving inside a metal [15], has not yet been presented.

In this paper, we will concentrate on some of the mechanisms of electron-hole (e-h) excitation. First, we will derive the excitation probability in terms of the screened potential. The production of e-h pairs induced by a charged projectile will be studied both in the homogeneous electron gas and near surfaces. A description of screening at surfaces will be given as well. Finally, the spatial representation of e-h pair production will be discussed.

Some of the basic features that characterize the emission of electrons in solids can be understood by analyzing their spectrum of electronic excitations, represented in Figure 1. Figure 1a corresponds to the homogeneous electron gas. The dashed region represents allowed transitions between free electron states. The shaded region shows the electronic excitations of the

Symbol Table

E_F	Fermi energy
$f_{\mathbf{k}}$	Occupation probability of state $\mathbf{k}$
$\mathbf{j}$, $\mathbf{j}^i$, $\mathbf{j}^e$	Total charge current, induced charge current, external charge current
J_0, J_1	Bessel functions of 0^{th} and first order
$\mathbf{k}$, $\mathbf{q}$	Momentum vectors
$\mathbf{K}_\parallel$, $\mathbf{Q}$	Components of the momentum vectors parallel to the surface
K_0, K_1	Modified Bessel functions of 0^{th} and first order
N	Ratio between coincidence counts and electron energy loss spectroscopy (EELS) counts
P	Probability per incoming particle
$\mathbf{r}$	Spatial coordinate
r_s	One-electron radius
R	Distance to the trajectory of the particle
S	Stopping power
S^h, S^e, S^{pl}	Stopping power associated to holes, electrons, and plasmons
t	Time
V_0	Height of the surface barrier
$\mathbf{v}$	Particle velocity
v_F	Fermi velocity
W, W^i	Screened interaction, induced part of the screened interaction
γ	Damping
Γ	Probability per incident particle per unit time
$\epsilon(k,\omega)$	Dielectric function
$\epsilon_s(Q,z,\omega)$	Surface dielectric function
$\hbar\epsilon_{\mathbf{k}}$	Energy of state $\mathbf{k}$
ρ, ρ^i, ρ^e	Charge density
ϕ, ϕ^i, ϕ^e	Screened potential, induced potential, external potential
χ	Polarizability
χ_0	Polarizability in the random-phase approximation
$\psi_{\mathbf{k}}$	Wave function of state $\mathbf{k}$
ϕ_{k_z}	Wave function in the z direction
$\Omega_{\mathbf{q}}$	Solid angle around the direction given by $\mathbf{q}$
ω	Frequency of an elemental excitation
ω_p	Bulk plasmon frequency
ω_s	Surface plasmon frequency

media that can be induced by an infinite mass particle moving with velocity v. The self-consistency of the response is translated into the emergence of collective excitations, the bulk plasmons. The plasmon line has been broadened in the figure to indicate that these collective modes can decay, giving rise to further e-h pairs. The decay of bulk plasmons is forbidden in a non-interacting free electron gas, except at the resonance point labeled C in the figure [4]. It has been shown that the main mechanism of plasmon decay consists in transferring momentum to the lattice in order to fulfill the momentum and energy conservation, that is, via inter-band transitions [8, 65].

Electron transitions are also made possible when the translational symmetry of the medium is broken. That is the case in homogeneous surfaces, where the excitation spectrum is better understood in terms of parallel momentum transfer, $\hbar Q$, as shown in Figure 1b. The resulting collective modes are the surface plasmons, first predicted by Ritchie [52]. It has been shown that bulk and surface plasmons approach the same point C for large momentum [33] (Fig. 1). Notice that the e-h pair region includes most of the Q-ω plane, and overlaps the plasmon line. In other words, since the electrons are no longer free due to the presence of the surface, surface plasmons can decay by inducing intra-band transitions, unlike what happens with bulk plasmons. A study of the relative importance of intra- and inter-band transitions in the decay of surface plasmons is still lacking.

The perturbation generated in the medium by an external charge will be described in terms of the classical external potential throughout this work. This constitutes a reasonable approximation for ions or hot electrons. That is not the case for low-energy electrons, where the Pauli exclusion principle must be taken into account, in the sense that not all of the excitations in the shaded region of Figure 1a are allowed. This fact has been considered in a nice theoretical development, due to Ritchie and coworkers [54, 56, 62], who calculated the flux of coupled electrons and holes in the low energy end, finding remarkable agreement with experiment.

Atomic units (a.u.), in which $m = \hbar = e^2 = 1$, will be used in some of the figures. More precisely, a velocity of v = 1 a.u. corresponds to approximately 25 keV-H^+ or 13.6 eV-e^- projectiles.

Electron-Hole Pair Excitation Probability

We will express the perturbation introduced by the external probe in the medium in terms of the external scalar potential $\phi^e(\mathbf{r},t)$. The energy transferred to the medium by this perturbation can in turn be translated into the production of e-h pairs. The probability of e-h pair creation will be derived below following these considerations, within the framework of linear response theory. The random-phase approximation (RPA) will be invoked eventually, which means that the solid will be described as a set of independent electrons that respond to the self-consistently-screened external field.

The density of energy deposited per unit time at the position $\mathbf{r}$ can be expressed in terms of the work exerted by the screened electric field $-\nabla\phi(\mathbf{r},t)$ acting on the induced charge current $\mathbf{j}^i(\mathbf{r},t)$ as

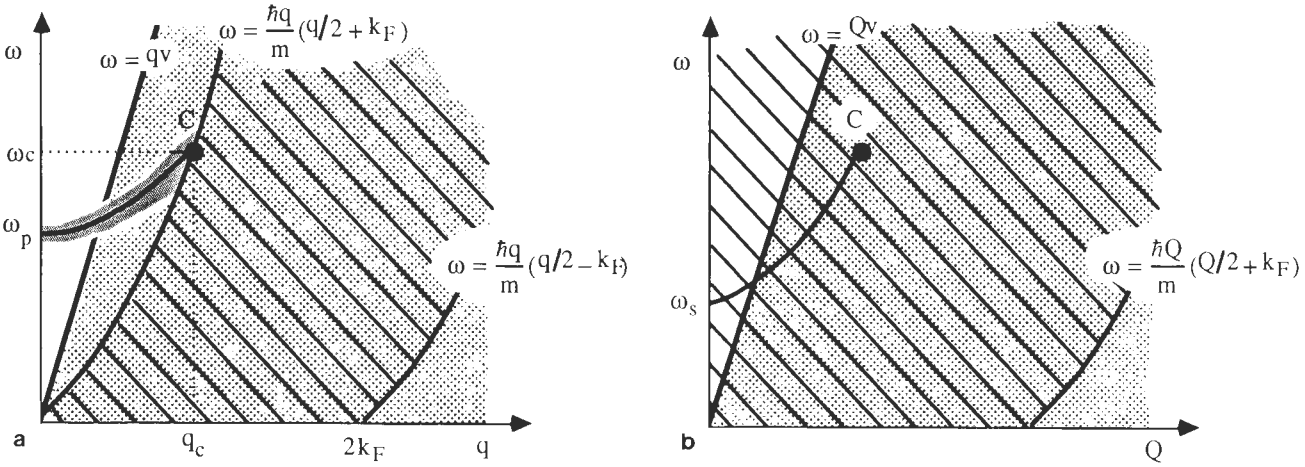

Figure 1. (**a**) Schematic representation of the spectrum of excitations in a homogeneous electron gas. $\hbar q$ and $\hbar\omega$ represent the momentum and energy transfers, respectively. $\hbar k_F$ is the Fermi momentum. ω_p is the classical plasma frequency. The dashed region corresponds to allowed electron-hole pair excitations. The shaded region stands for electronic excitations that can be created by an infinite mass particle moving with velocity v. (**b**) The same as (a) for a homogeneous surface. $\hbar Q$ represents the component of the momentum transfer parallel to the surface. ω_s is the classical surface plasma frequency.

$$\frac{dE}{drdt} = -\boldsymbol{j}^{i}(\boldsymbol{r},t)\cdot\nabla\phi(\boldsymbol{r},t)\,. \tag{1}$$

It is important to use the screened potential $\phi(\mathbf{r},t)$, rather than the external potential in eq. (1), since the induced part of the potential plays the role of redistributing the deposited energy. Integrating eq. (1) over $\mathbf{r}$ by parts and using the continuity equation, it is easy to prove that the induced potential contributes with a conservative work.

The total energy loss is obtained from eq. (1) by integrating over $\mathbf{r}$ and t. Using the procedure just described, one finds

$$E = \int_0^\infty d\omega\hbar\omega\frac{dP}{d\omega}\,,$$

where

$$\frac{dP}{d\omega} = -\frac{1}{\pi\hbar}Im\left\{\int d^3r\int d^3r'\phi^*(\boldsymbol{r},\omega)\cdot \chi_0(\boldsymbol{r},\boldsymbol{r}',\omega)\phi(\boldsymbol{r}',\omega)\right\} \tag{2}$$

is the probability distribution for delivering energy $\hbar\omega$ to the medium, $\phi(\mathbf{r},\omega)$ is the time-Fourier transform of $\phi(\mathbf{r},t)$, and $\chi_0(\mathbf{r},\mathbf{r}',\omega)$ is the electric polarizability. Then, one can express the induced charge $\rho^i(\mathbf{r},t)$ in terms of the screened potential as

$$\rho^{i}(\boldsymbol{r},\omega) = \int d^3r'\chi_0(\boldsymbol{r},\boldsymbol{r}',\omega)\phi(\boldsymbol{r},\omega)\,.$$

Eq. (2) is exact within the linear response approximation, provided one knows the exact polarizability. The latter reads, in the RPA,

$$\chi_0(\boldsymbol{r},\boldsymbol{r}',\omega) = \frac{2e^2}{\hbar}\sum_{k,k'}(f_k - f_{k'})\frac{\psi_k^*(\boldsymbol{r})\psi_{k'}(\boldsymbol{r})\psi_{k'}^*(\boldsymbol{r}')\psi_k(\boldsymbol{r}')}{\varepsilon_k-\varepsilon_{k'}+\omega+i\gamma}, \quad \gamma\to 0^+, \tag{3}$$

where $\psi_k(\mathbf{r})$ represents a spatial basis set eigenfunction of energy $\hbar\epsilon_k$ and occupation probability f_k, and the factor of 2 arises from the summation over electron spin.

It is convenient to rearrange eq. (3) so that it contains the expression $f_{k'}(1-f_k)$. In this way, the corresponding term refers to an electron in the state ψ_k and a hole in the state $\psi_{k'}$. Then, inserting eq. (3) into eq. (2), one obtains

$$\frac{dP}{d\omega} = \sum_{k,k'}\frac{dP_{k,k'}}{d\omega}, \tag{4}$$

where

$$\frac{dP_{k,k'}}{d\omega} = \frac{2e^2}{\hbar^2}f_{k'}(1-f_k)\cdot |\langle k|\phi|k'\rangle|^2\delta(\varepsilon_k-\varepsilon_{k'}-\omega) \tag{5}$$

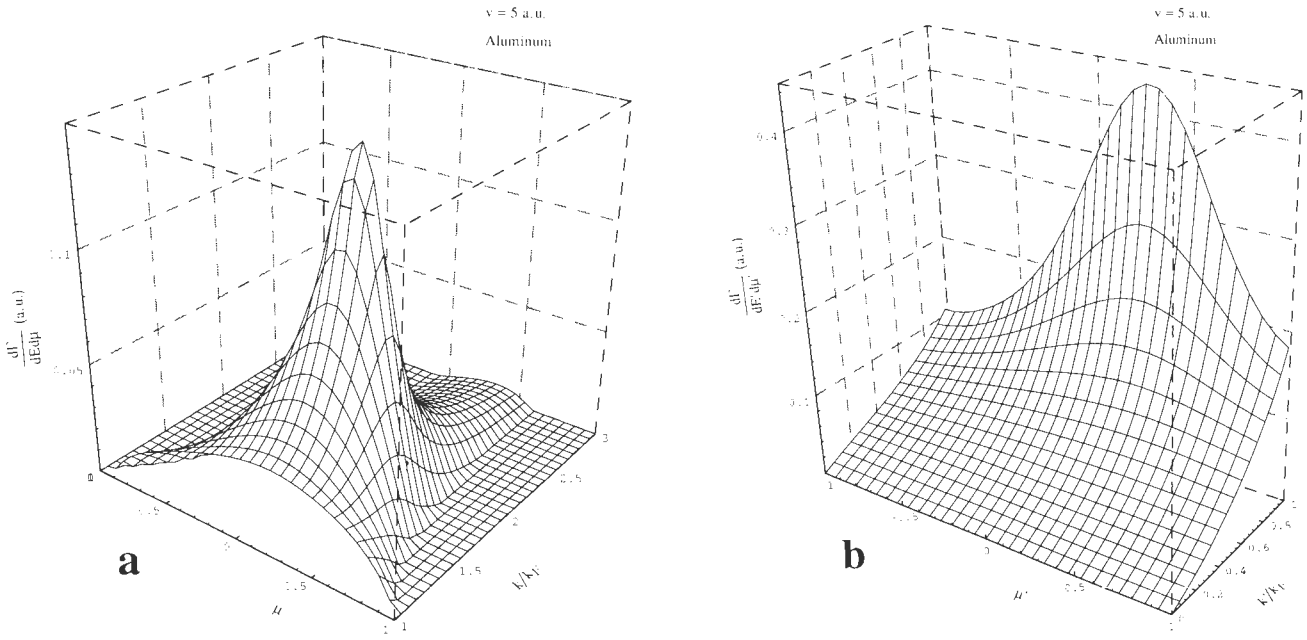

Figure 2. (**a**) Doubly differential electron excitation rate due to the interaction of a homogeneous electron gas with a unit charge moving with constant velocity v = 5 a.u., according to eq. (7). The momentum and direction of motion of the electron are given by $\hbar$k and $\mu = \cos(\mathbf{k},\mathbf{v})$, respectively. The Mermin dielectric function [40] has been used to represent the response of the medium. Electron gas parameters appropriate to aluminum have been utilized (one-electron radius $r_s = 2.07\ a_0$ and damping $\hbar\gamma = 1.35$ eV). (**b**) Under the same conditions, creation rate of holes of momentum $\hbar$k' around the direction $\mu' = \cos(\mathbf{k}',\mathbf{v})$, according to eq. (8).

---

is the probability of creating an e-h pair of frequency $\omega = \epsilon_k - \epsilon_{k'}$. The matrix element in this equation reads

$$\langle k|\phi|k'\rangle = \int d^3r \psi_{k}^{*}(r)\phi(r,\omega)\psi_{k'}(r) .$$

Eq. (5) is the Fermi golden rule for a perturbation described by the screened potential ϕ.

Electron Excitation in Homogeneous Media

In this section, we shall consider that the external perturbation is provided by a charged particle of charge eZ_1 moving with constant velocity v in a homogeneous gas of independent electrons. Then, the perturbing screened potential is the well-known wake potential [13, 15, 45, 46]. Performing partial summations in eq. (4), one obtains different quantities of interest. For instance, summing only over the holes **k'** and integrating over ω, one finds the electron excitation probability. This function was first studied for the homogeneous electron gas by Ritchie [53], who showed that this result is the same as that obtained from the self-energy method [15]. An exhaustive comparison between this result and the Rutherford scattering of an electron gas by the bare Coulomb potential can be found in reference [4].

We will take the states ψ_k as plane waves of momentum $\hbar$**k**. Since eq. (4) is the total probability, we need to divide it by the interaction time in order to get transition rates. This can be done by considering that the screened potential is switched on (off) at the finite time t = -a (t = a), so that, for a point charge Z_1e moving at constant velocity **v**,

$$\langle k|\phi|k'\rangle = \frac{2Z_1 W(q,\omega)}{\Omega}\frac{\sin[(\omega-\mathbf{q}\cdot\mathbf{v})a]}{\omega-\mathbf{q}\cdot\mathbf{v}} .$$

Here, Ω is the normalization volume, $\mathbf{q} = \mathbf{k}-\mathbf{k}'$ is the momentum transfer, and

$$W(q,\omega) = \frac{4\pi e^2}{q^2\varepsilon(q,\omega)}$$

is the screened interaction, expressed in terms of the dielectric function $\epsilon(q,\omega)$. Taking the $a \to \infty$ limit, the differential transition rate is found to be

$$\frac{d\Gamma}{d\omega d\mathbf{k} d\mathbf{k}'} = \lim_{a\to\infty}\frac{1}{2a}\frac{dP}{d\omega d\mathbf{k} d\mathbf{k}'}$$

$$= \frac{Z_1^2 e^4}{\hbar^2\pi^3} f_{k'}(1-f_k)\frac{1}{|q^2\varepsilon(q,\omega)|^2}$$

$$\cdot\,\delta(\omega-\mathbf{q}\cdot\mathbf{v})\,\delta(\varepsilon_k-\varepsilon_{k'}-\omega) \qquad (6)$$

where we have made use of the identity [41]

$$\lim_{a\to\infty}\frac{\sin^2 ax}{ax^2} = \pi\delta(x).$$

Integrating eq. (6) over ω and all possible hole states $\mathbf{k}'$, one finds the differential electron excitation rate

$$\frac{d\Gamma^e}{dEd\mu} = \frac{4m^2Z_1^2e^4k}{\pi^2\hbar^4}\cdot\int_{(E-E_F)/(\hbar v)}^{k\mu-mv/\hbar+|\mathbf{k}-m\mathbf{v}/\hbar|}d\zeta \times\int_0^{\pi/2}d\varphi\frac{1}{|q^2\varepsilon(q,\zeta v)|^2},$$
$$\text{for } |v-v_F|<|\hbar\mathbf{k}/m-\mathbf{v}|<v+v_F,$$
$$= 0, \text{ for rest} \qquad (7)$$

where $\mu = \cos(\mathbf{k},\mathbf{v})$,

$$q^2 = 2\left[k^2(1-\mu^2)+\zeta(k\mu-mv/\hbar) - k\cos\varphi\sqrt{1-\mu^2}\cdot\sqrt{|\mathbf{k}-m\mathbf{v}/\hbar|^2-(k\mu-mv/\hbar-\zeta)^2}\right],$$

v_F and E_F are the Fermi velocity and energy, respectively, and we have replaced the electron energy $\hbar\epsilon_{\mathbf{k}}$ by E.

Figure 2a represents the dependence of the electron excitation rate on momentum and angle for a unit charge particle moving with constant velocity v = 5 a.u. inside aluminum. The RPA dielectric function [36] has been used, together with the Mermin prescription [40], which permits the use of finite values of the electron gas damping parameter while maintaining the number of electrons in the medium constant. The spectrum of excited electrons is characterized by a peak in the k-μ plane [4]. This peak comes from energy-momentum transfers around the resonance point C of coordinates (q_c,ω_c) (Fig. 1a). The position of the peak is given by $k_c = 2m\omega_c/\hbar q_c - k_F$ and $\mu_c = \omega/qv$, where $\hbar k_F$ is the Fermi momentum (in aluminum, this corresponds to electrons of 35.3 eV).

Similarly, integrating eq. (6) over $\mathbf{k}$, one obtains the energy and angle distribution of holes

$$\frac{d\Gamma^h}{dE'd\mu'} = \frac{4m^2Z_1^2e^4k}{\pi^2\hbar^4}\cdot\int_{(E_F-E')/\hbar v}^{mv/\hbar-k'\mu'+|\mathbf{k}'-m\mathbf{v}/\hbar|}d\zeta\cdot\int_0^{\pi/2}d\varphi\frac{1}{|q^2\varepsilon(q,\zeta v)|^2}, \qquad (8)$$

where $\mu' = \cos(\mathbf{k}',\mathbf{v})$,

$$q^2 = 2\left[k'^2(1-\mu'^2)+\zeta(mv/\hbar-k'\mu') - k'\cos\varphi\sqrt{1-\mu'^2}\cdot\sqrt{|\mathbf{k}'-m\mathbf{v}/\hbar|^2-(mv/\hbar-k'\mu'-\zeta)^2}\right],$$

and $E' = \hbar\epsilon_{\mathbf{k}'}$.

Figure 2b shows that most of the electrons are excited from the region near the Fermi level (i.e., most of the holes are left there). The holes are preferentially created roughly around the same direction observed above for electrons. This anisotropy should be considered when analyzing the cascade of e-h pairs originated in the passage of swift charges through an electron gas. The relative importance of holes in the cascade will be discussed later by analyzing the fractions of energy carried by electrons and holes.

Screening at the Surface

Part of this work is concerned with electron excitation at surfaces. To do this one needs to know how to calculate the screened potential ϕ near the surface. The present section is devoted to the study of the features that characterize the screened potential created by an external moving charge in the vicinity of a homogeneous solid surface. The so-called surface wake potential [21, 22, 23] can be expressed in terms of the screened interaction W as

$$e\phi(\mathbf{r},t) = \int\frac{d^2Qd\omega}{(2\pi)^3}e^{i(\mathbf{Q}\cdot\mathbf{R}-\omega t)}\cdot\int dz'W(Q,z,z',\omega)\rho^e(\mathbf{Q},z',\omega), \qquad (9)$$

where some magnitudes are expressed in the space of Fourier transformations with respect to the directions parallel to the surface and the time {i.e., $(\mathbf{Q},z,\omega)$}. Upper-case vectors will be reserved for components parallel with the surface from now on.

The complexity of the surface response requires one to adopt strong assumptions in order to make it numerically tractable without employing extensive computer calculations. The specular-reflection model of Ritchie and Marusak [58] provides an approximation to the problem that has the virtue of incorporating dispersion effects by expressing the surface response in terms of the bulk dielectric function. In this model, the medium is described by a 'jellium,' in which the surface is assumed to be abruptly terminated; the electrons forming the response of the medium are considered to be specularly reflected at the surface. Thus, the electronic charge density vanishes outside the surface. The screened interaction takes the form

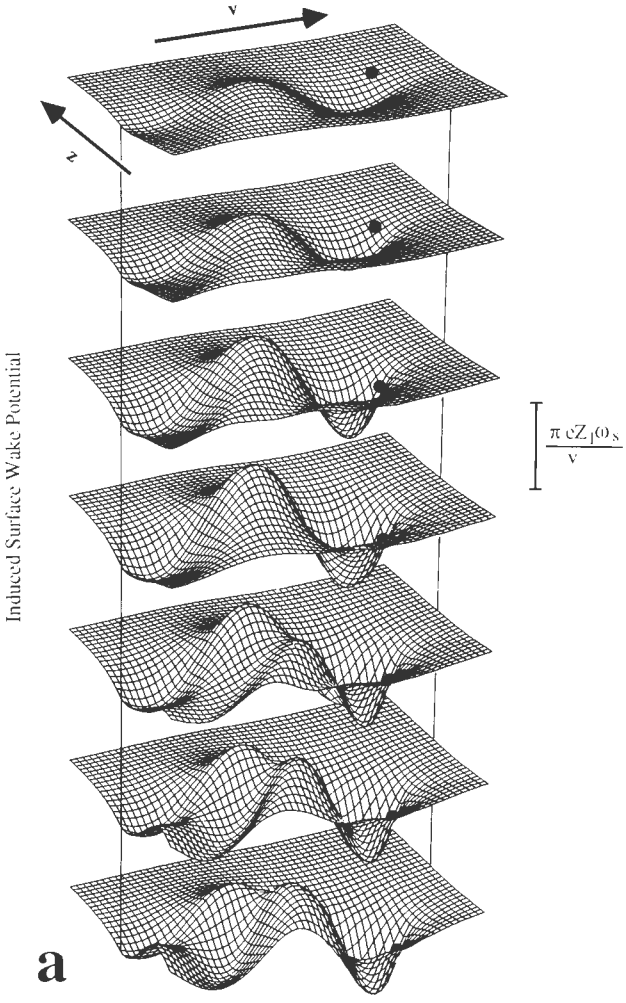

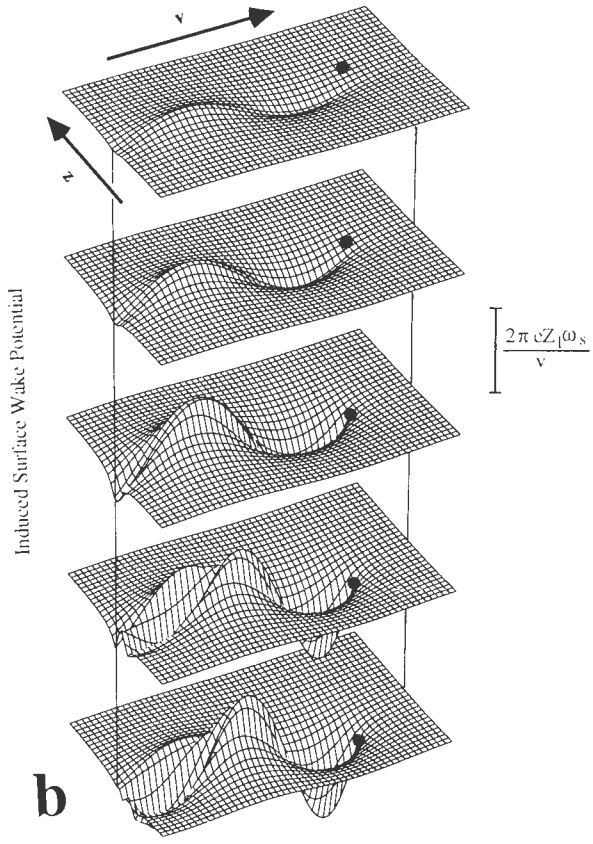

Figure 3. (**a**) Induced surface wake potential created by a charged particle of charge eZ_1 moving with constant velocity v = 2 a.u. parallel to an aluminum surface for various impact parameters: $z_0\lambda$ = 0.4, 0.2, 0, -0.2, -0.4, -0.6, and -0.8 (from top to bottom), where $\lambda = \pi v/2\omega_s$ (= 4.04 Å). Eqs. (10), (11), and (12) have been used. The surface, represented by vertical lines, is placed at z = 0. The vacuum occupies the z > 0 region. Each grid extends from z = -λ to z = λ along the surface normal, and from x = -4λ to x = λ along the direction of motion. The subdivisions in the grids correspond to squares of side λ/10. The particle (black circles) is located at x = 0 and moving from left to right. (**b**) The same as (a) for a larger value of the velocity, v = 10 a.u. (λ = 20.2 Å), and z_0/λ = 0.4, 0.2, 0, -0.2, and -0.4.

$$
\begin{aligned}
W(Q,z,z',\omega) &= \frac{2\pi e}{Q} \\
&\times \frac{\varepsilon_s(Q,\omega)-1}{\varepsilon_s(Q,\omega)+1} e^{-Q(z+z')} + e^{-Q|z-z'|}, \\
&\quad \text{for } z\geq 0,\ z'\geq 0; \\
&\times \frac{2\varepsilon_s(Q,z,\omega)}{\varepsilon_s(Q,\omega)+1} e^{-Qz'}, \quad \text{for } z<0,\ z'\geq 0; \\
&\times \frac{2\varepsilon_s(Q,z',\omega)}{\varepsilon_s(Q,\omega)+1} e^{-Qz}, \quad \text{for } z\geq 0,\ z'<0; \\
&\times \varepsilon_s(Q,z-z',\omega) + \varepsilon_s(Q,z+z',\omega) \\
&\quad - \frac{2\varepsilon_s(Q,z',\omega)\,\varepsilon_s(Q,z,\omega)}{\varepsilon_s(Q,\omega)+1}, \\
&\quad \text{for } z<0,\ z'<0;
\end{aligned}
\tag{10}
$$

where

$$
\varepsilon_s(Q,z,\omega) = \frac{Q}{\pi}\int_{-\infty}^{\infty} \frac{dk_z}{k^2} \frac{e^{ik_z z}}{\varepsilon(k,\omega)}
$$

is the so-called surface dielectric function, first used by Newns [47], and we have taken the vacuum in the z > 0 region and $k = (Q^2+k_z^2)^{1/2}$. The response in the vacuum is dominated by surface plasmon terms, as seen in eq. (10). The poles $\epsilon_s(Q,\omega) + 1 = 0$ in those terms

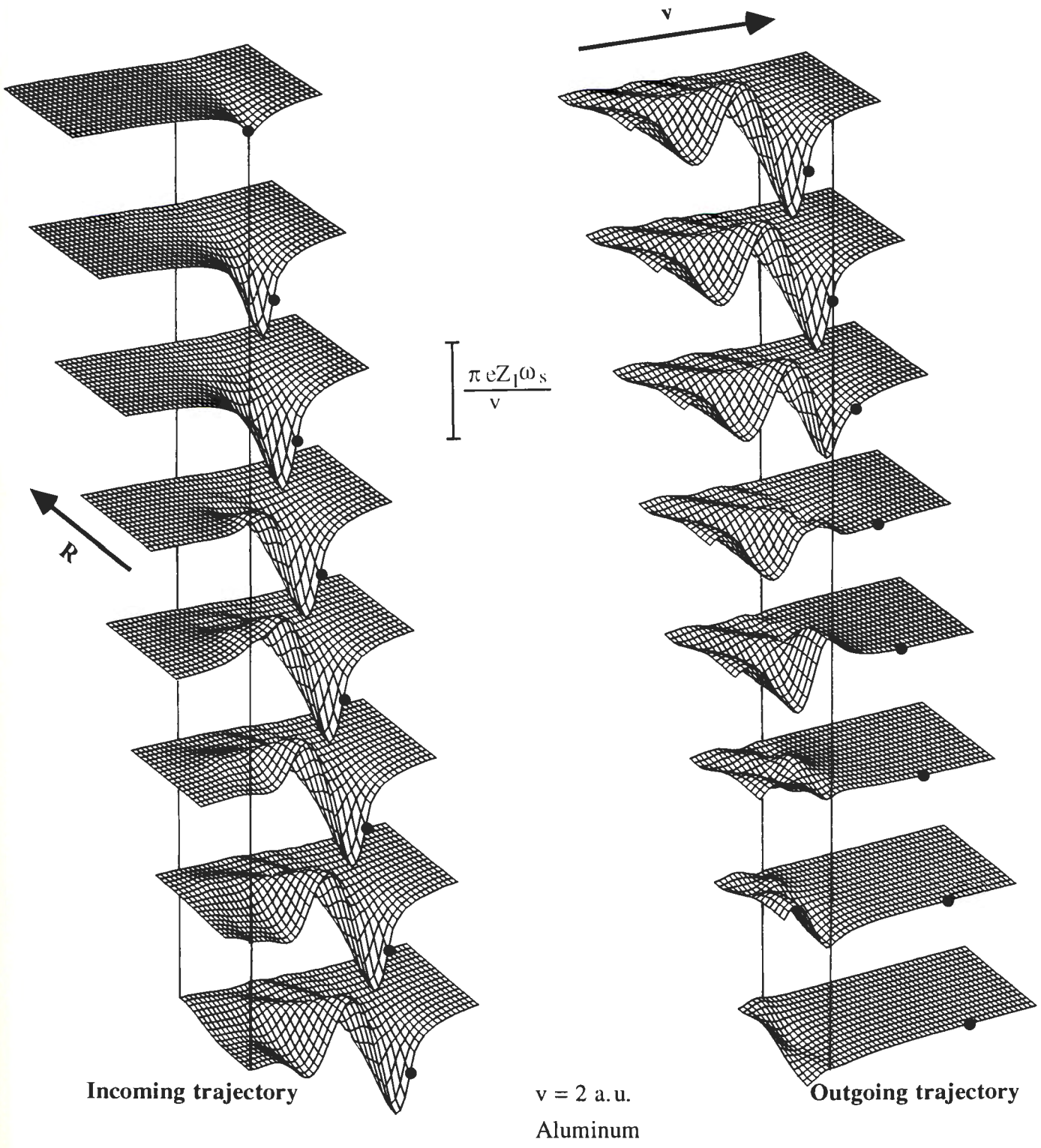

Figure 4. Induced surface wake potential created by a charged particle of charge eZ_1 moving with constant velocity v = 2 a.u. perpendicular to an aluminum surface for the cases of incoming (left) and outgoing (right) trajectories. The surface is represented by vertical lines, with the medium located on the right/left side in the incoming/outgoing trajectory. The dimensions of each grid are 50x15 a.u. (i.e., 26.4 x 7.9 Å). The subdivisions in the grids correspond to squares of side 1 a.u. The particle (black circles) is moving from left to right. R is the direction perpendicular to the trajectory.

define the possible self-sustained collective excitations in the surface; that is, they provide the surface plasmon dispersion relation [58], schematically shown in Figure 1b. Although more sophisticated treatments are necessary to describe a real surface, the specular-reflection model has found wide application when one needs to characterize the complete response function of a bounded metal, as in the calculation of the image potential [7, 19, 26, 30], the energy loss of fast charges moving near solid surfaces [31, 35, 48] and the surface wake potential. The latter has been obtained using different approximations to the dielectric functions: the local response [64, 71], the hydrodynamic approximation [17, 21], the plasmon pole approximation [22] and the full random-phase approximation [23, 27].

For a charge eZ_1 traveling parallel to the surface with constant velocity $\mathbf{v}$ and impact parameter z_0, the external charge density reads

$$\rho^e(\mathbf{Q},z,\omega) = 2\pi eZ_1\delta(\omega-\mathbf{Q}.\mathbf{v})\delta(z-z_0),$$

and accordingly,

$$\phi(\boldsymbol{r},t) = Z_1\int\frac{d^2Q}{(2\pi)^2}e^{i\boldsymbol{Q}\cdot(\boldsymbol{R}-\boldsymbol{v}t)}W(Q,z,z_0,Q\cdot v)\,. \tag{11}$$

Figure 3 represents the induced surface wake potential, calculated from eqs. (10) and (11), for a charge moving with velocity (a) v = 2 a.u. and (b) v = 10 a.u. parallel to an aluminum surface. The projectile position is indicated by black circles. The plasmon-pole approximation has been used for the bulk dielectric function [38], in which case

$$\varepsilon_s(Q,z,\omega) = \frac{\omega(\omega+i\gamma)}{\Omega}e^{-Q|z|} + \frac{Q\omega_p^2}{\Lambda_+-\Lambda_-}\left\{\frac{e^{-|z|R_-}}{\Lambda_-R_-}-\frac{e^{-|z|R_+}}{\Lambda_+R_+}\right\}, \tag{12}$$

where:

$\Omega = \omega(\omega+i\gamma)-\omega_p^2$;

$\Lambda_\pm = m\beta^2/\hbar \pm \{(m\beta^2/\hbar)^2+\Omega\}^{1/2}$; and

$\beta = (3/5)^{1/2}v_F$ is the velocity of propagation of disturbances in the medium, $R_\pm = (Q^2+2m\Lambda_\pm/\hbar)^{1/2}$, and the square root is understood to yield positive real parts.

The excitation of surface plasmons is translated into oscillations of frequency ω_s in the potential. This happens only when the external charge moves near the surface, that is, at distances smaller than the characteristic length of screening of the surface wake potential v/ω_s. Bulk plasmons do not show up when the particle travels inside the medium close to the surface. As the ion moves deeper inside the material, surface plasmon oscillations slowly fade off, giving way to oscillations of frequency characteristic of bulk plasmons. In the specular-reflection model used here, the latter only appear in the potential when the particle travels a few Å below the surface. More sophisticated models for the surface response allow for the "penetration" of bulk plasmons in the vacuum region [16].

When the particle moves along a straight line, the external charge density takes the form $\rho^e(\mathbf{r},t) = eZ_1\delta(\mathbf{r}-vt)$. Inserting this expression into eq. (9), and using eq. (10), one can study the surface wake potential for trajectories that cross the surface [22, 23]. This case is contemplated in Figure 4, where the projectile is taken to move along the surface normal, both towards the solid (left) and away from it (right), with velocity v = 2 a.u. The plasmon pole dielectric function [38] has been used to describe the bulk material. The wake potential creation and destruction processes can be clearly observed in the figure. In the outgoing case, the wake remains almost unchanged until the particle reaches the surface. The potential at the position of the charge is approximately given by $-eZ_1\pi\omega_s/2v$ when it is at the surface, which is a value in-between the bulk limit, $-eZ_1\pi\omega_p/2v$, and the classical induced potential asymptote, $-eZ_1/4z$, valid at large distances z from the solid.

The Loss Function

Summing over all electrons and holes in eq. (5), one gets back the probability of creating excitations of frequency ω in the medium {eq. (2)}. A more convenient expression for this quantity can be obtained by invoking the conservation of energy, which leads to the conclusion that the energy deposited in the medium equals minus the energy expended in moving the charge against the induced electric field, i.e.,

$$\frac{dE}{drdt} = j^e(\boldsymbol{r},t)\cdot\nabla\phi^i(\boldsymbol{r},t)\,.$$

Starting from this instead of eq. (1), and following the procedure indicated below that equation, one obtains

$$\frac{dP}{d\omega} = \frac{1}{\pi\hbar}Im\left\{\int d^3r\phi^i(\boldsymbol{r},-\omega)\rho^e(\boldsymbol{r},\omega)\right\}.$$

This expression can be worked out for a particle traveling parallel to a solid surface with the help of eq. (11). Dividing by the total interaction time, in a way similar to that shown in eq. (6), the probability of creating an excitation of energy $\hbar\omega$ in the medium per incident particle per unit time is found to be

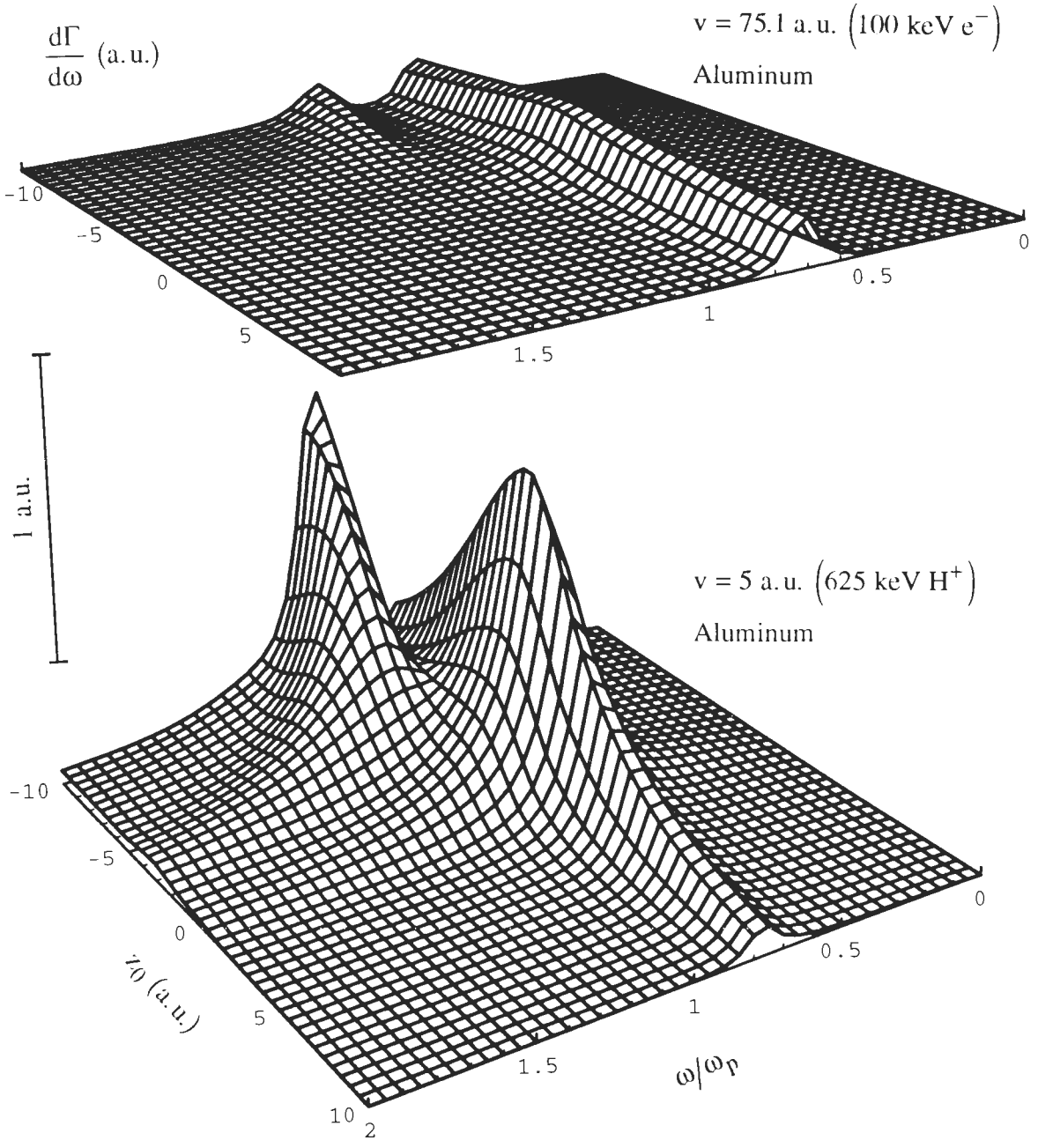

Figure 5. Creation rate of excitations of frequency ω induced by unit charge particles traveling parallel to an aluminum surface with impact parameter z_0 and different velocity regimes (see text in figure). $z_0 < 0$ means inner trajectories. The specular-reflection model has been used together with the Mermin dielectric function [40] {eqs. (10) and (13)}.

$$\frac{d\Gamma}{d\omega} = \frac{Z_1^2 e}{\pi^2 \hbar v} \int_0^\infty dQ_\perp \, Im\left\{-W^i(Q, z_0, z_0, \omega)\right\}, \tag{13}$$

where $Q = (Q_\perp{}^2 + \omega^2/v^2)^{1/2}$. For high velocity electrons, this probability can be measured by using STEM techniques [9, 32, 39]. One finds good agreement with experiment [14, 37, 76]. Good agreement is also obtained when considering more complex target geometries [18, 63]. The question of the extreme spatial sensitivity of this technique has been addressed by Ritchie *et al.* [55, 57, 60, 61] by analyzing the impact parameter representation of the inverse electron mean free path, obtained from eq. (13) as $\lambda^{-1} = v\Gamma$. This procedure will be extended below in order to obtain a spatial representation of the e-h creation probability.

In the local response approximation, eq. (13) reduces to the well-known expression [12, 48, 76]

$$\frac{d\Gamma}{d\omega} = \frac{2(eZ_1)^2}{\pi\hbar v} \cdot \left\{ K_0\left(\frac{2\omega|z_0|}{v}\right) Im\left\{\frac{\varepsilon(\omega)-1}{\varepsilon(\omega)+1}\right\} + \left[\ln\left(\frac{q_c v}{\omega}\right) - K_0\left(\frac{2\omega|z_0|}{v}\right)\right] \cdot Im\left\{\frac{-1}{\varepsilon(\omega)}\right\}\theta(-z_0)\right\}, \quad (14)$$

where K_0 is the modified Bessel function of the second kind, $\epsilon(\omega)$ is the local dielectric function of the material, and q_c is a momentum cutoff, usually chosen to correspond to point C in Figure 1a. This expression was apparently first given by Núñez *et al.* [48]. The first term in the above expression represents losses due to the excitation of surface modes [12, 52], while the last term corresponds to bulk losses. The logarithmic term modifies the bulk losses in the sense of inhibiting them in the region near the surface. The expression inside square brackets exactly vanishes at the surface if one corrects the logarithmic divergence of the K_0 function by employing a finite momentum cutoff q_c. This is the boundary effect, predicted by Ritchie [52] and named "begrenzung" later [3].

Figure 5 shows $d\Gamma/d\omega$ for a unit charge projectile moving near aluminum, calculated using the specular-reflection model and the Mermin dielectric function [40]. Two different velocity regimes have been studied. The bulk plasmon losses dominate for negative impact parameters, that is, inside the solid, while the surface losses are more important near the surface region. The figure clearly shows the effect of begrenzung. The influence of the surface in the loss probability extends up to the characteristic screening length v/ω_s. This can be observed in Figure 5 by comparing the different projectile velocities under consideration: for large velocities (upper sheet), the surface plasmons play a relevant role even at large distances from the surface.

It is interesting to note that the surface losses concentrate near the surface plasma frequency ω_s both for large velocities and for large distances to the surface, that is, in the limits of validity of the local response approximation {eq. (14)}. For small velocities, the surface plasma losses occur at slightly larger frequencies in the near-the-surface region (see lower part of Fig. 5). This result is related to the fact that the surface plasmon dispersion is positive within the specular-reflection model used here {eq. (10)}.

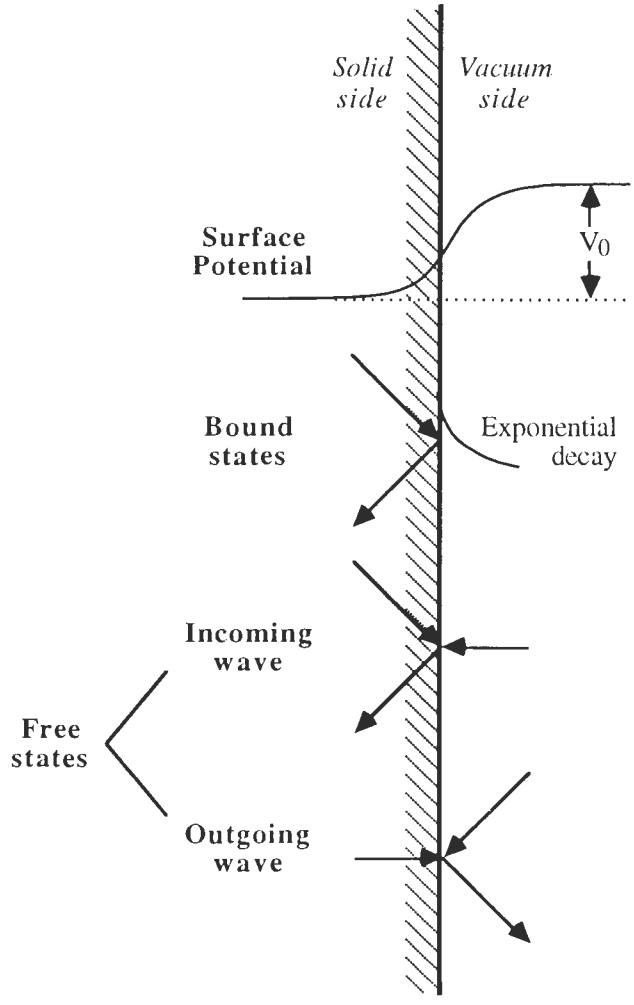

Figure 6. Schematic representation of the basis set of states used to calculate the ejection of electrons from a solid surface. The wave functions are solutions of the Schrödinger equation with the potential shown in the upper part of the figure. The arrows are intended to show the directions of the plane waves in terms of which the wave functions can be written for large distances from the surface, where the potential becomes flat.

Electron Excitation in Homogeneous Surfaces

The homogeneity of the surface guarantees that the one-electron states can be written in the form

$$\psi_k(\boldsymbol{r}) = \frac{e^{i\boldsymbol{K}_\parallel\cdot\boldsymbol{R}}}{\sqrt{A}}\varphi_{k_z}(z), \quad (15)$$

where A is the area of the surface and $\hbar k$ is the momentum in the solid side. Thus, $E = \hbar\epsilon_{\mathbf{k}} = (\hbar k)^2/2$ is the energy of the electron with respect to the bottom of the conduction band.

A complete basis of wave functions ϕ_{k_z} includes both bound states and free states, as Figure 6 illustrates in a schematic way. Since the process of electron emission involves the detection of electrons in the vacuum side, far from the surface, one has to use a suitable set of free states. The one depicted in Figure 6 has the virtue that only the outgoing wave states contribute to the direct emission [20], thus avoiding the complication of handling possible interferences between degenerate states at an infinite distance from the surface [74]. The states that we have actually employed to perform the numerical calculations discussed below are solutions of the Schrödinger equation for a square barrier potential.

The electrons are refracted at the surface, since they have to cross a potential barrier of height $V_0 = E_F + \Phi$ (Fermi energy + work function; see Fig. 6). We will denote $\hbar\mathbf{q}$ the momentum of the electron in the vacuum side, so that $\mathbf{Q}_\parallel = \mathbf{K}_\parallel$ and $q_z^2 = k_z^2 - 2mV_0/\hbar^2$.

Transport of excited electrons up to the surface will be accounted for through the simple procedure of multiplying the final state wave functions by an exponentially decaying function of the distance that the electron has to travel until it crosses the surface. The rate of decay is approximated by its value in the bulk of the material, expressed in terms of the mean free path of the excited electron, λ_k, according to

$$\varphi_{k_z}(z) \rightarrow \varphi_{k_z}(z)\exp\left[\frac{zk}{2\lambda_k k_z}\right], \quad z<0, \tag{16}$$

where the factor 1/2 in the exponent indicates that this attenuation is incorporated through the probability amplitude. For typical metals like aluminum, the electron inelastic mean free path has a minimum of some Å for electron energies of the order of 50 eV [1, 49, 59]. This should be compared with the screening length of the surface wake potential, v/ω_s. Thus, eq. (16) is valid for small velocities. Its range of validity is extended to larger velocities in the case of grazing trajectories, due to the fact that the length v/ω_s is an overestimate in the direction perpendicular to the surface, as can be seen in Figure 3b.

Before focusing in a particular orientation of the trajectory relative to the surface, let us rewrite eq. (5) for a homogeneous surface. One finds [24]

$$\frac{dP_{k_z}}{d\mathbf{K}_\parallel d\omega} = \frac{2e^2}{\hbar}(1-f_k)\int\frac{d^2K'_\parallel}{(2\pi)^4} \cdot \sum_{k'_z>0} f_{k'}\,|\langle k_z|\phi|k'_z\rangle|^2\,\delta(E-E'-\hbar\omega), \tag{17}$$

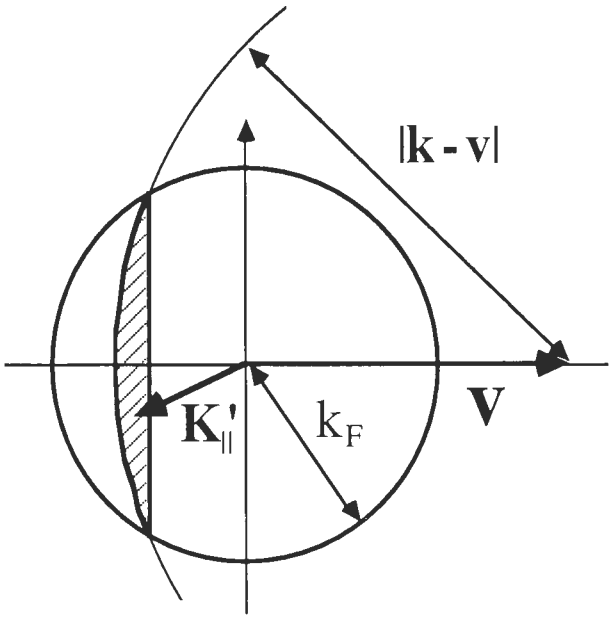

Figure 7. Domain of integration in eq. (18) in the $\mathbf{K'}_\parallel$-plane. $\hbar\mathbf{k}$ is the electron momentum inside the solid.

where

$$\langle k_z|\phi|k'_z\rangle = \int dz\,\varphi^*_{k_z}(z)\,\phi(Q,z,\omega)\,\varphi_{k'_z}(z),$$

$\mathbf{Q} = \mathbf{K}_\parallel - \mathbf{K'}_\parallel$ is the parallel momentum transfer, and $E' = \hbar\epsilon_{k'}$. Mills has derived this result using a technique similar to the one described above [42].

Grazing Incidence

When a charge eZ_1 moving along a straight line parallel to the surface with constant velocity $\mathbf{v}$ is considered, the time of interaction with the medium is infinite, and therefore, one has to follow a procedure similar to that which led to eq. (6) in order to convert the transition probability given by eq. (17) into a transition rate. After some algebra, the rate at which electrons are ejected with energy E around the solid angle $d\Omega_q$ is found to be, from eqs. (11) and (17) [24],

$$\frac{d\Gamma}{dEd\Omega_q} = \frac{2(meZ_1)^2 qq_z}{(2\pi)^3\hbar^5 k_z} \cdot \int\frac{d^2K'_\parallel}{k'_z}\theta(E_F-E')\,\theta(k^2-K'^2_\parallel-2m\omega/\hbar) \times|\langle k_z|W(Q,z,z_0,\omega)|k'_z\rangle|^2 \tag{18}$$

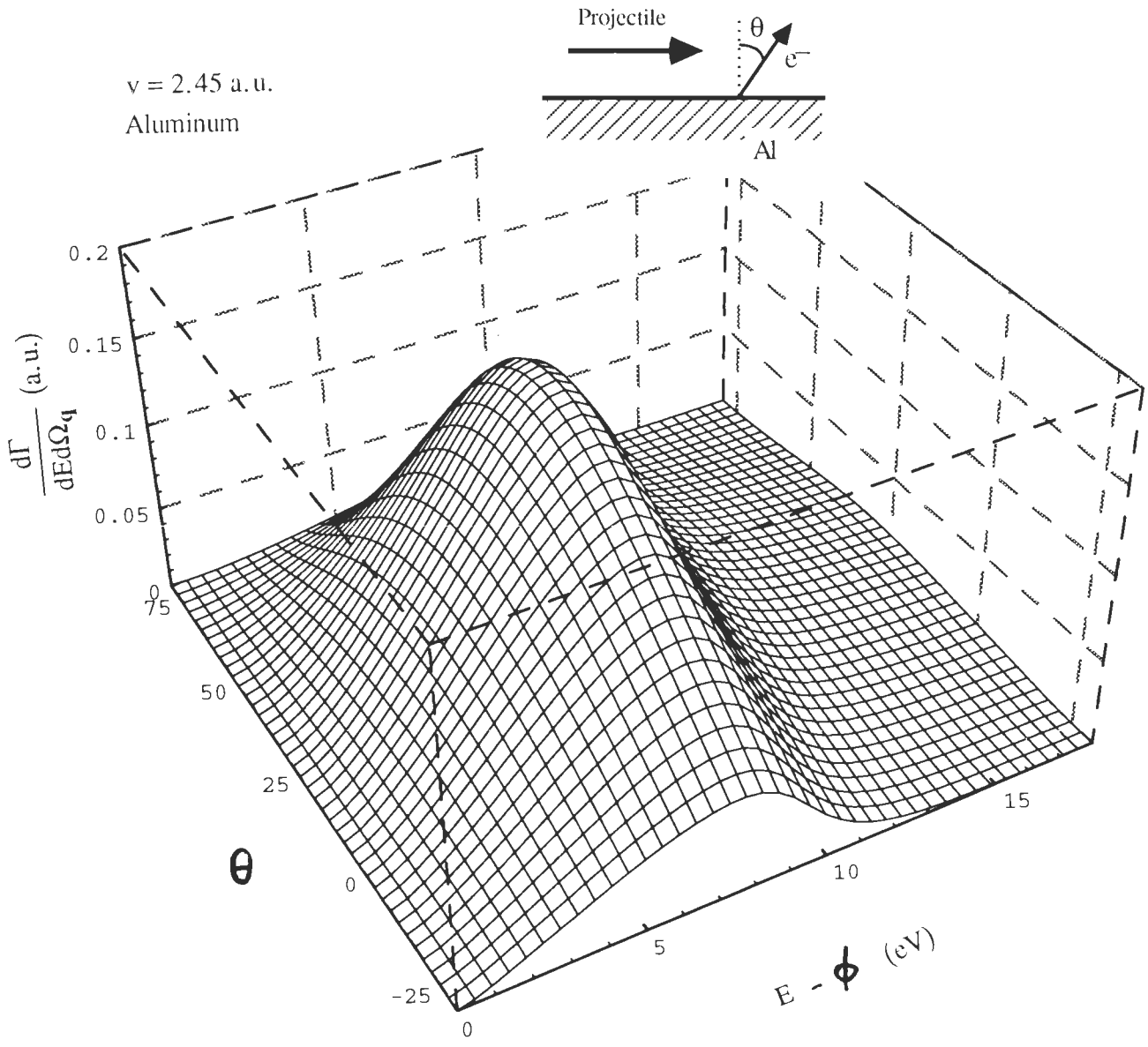

Figure 8. Differential rate of electron emission induced by a 150 keV-H^+ moving parallel to an aluminum surface at the surface edge. The angle θ determines the direction of emission in the plane given by the trajectory and the surface normal (see inset).

---

where $k'^2_z = k^2 - K'^2_{\parallel} - 2m\omega/\hbar$, ω = **Q.V.**, and δ-function normalization is used in the z-direction. The integral in eq. (18) is restricted to the dashed region shown in Figure 7.

Figure 8 shows the differential emission rate induced by a 150 keV proton, calculated from eq. (18), using the response function given by eq. (10) and the Mermin dielectric function [40]. The projectile trajectory is placed right in the surface. No significant difference is observed when the values of the mean free path λ_k introduced in eq. (16) are allowed to vary in the range typical for the electron energies under consideration [59]. The figure shows that the electrons are preferentially emitted in the forward direction, in qualitative agreement with recent experimental results [29].

The main feature observed in Figure 8 is the peak in the energy spectrum at the position $\hbar\omega_s - \phi$. This peak is formed by electrons which are excited from the top of the Fermi sea when a surface plasmon mediates in the process. Notice that within the specular-reflection model used here, the induced charge is confined below the surface. Inclusion of a more realistic description of the surface response [16] has been shown to result in the excitation of bulk plasmons even when the external ion moves in the near-surface region [25].

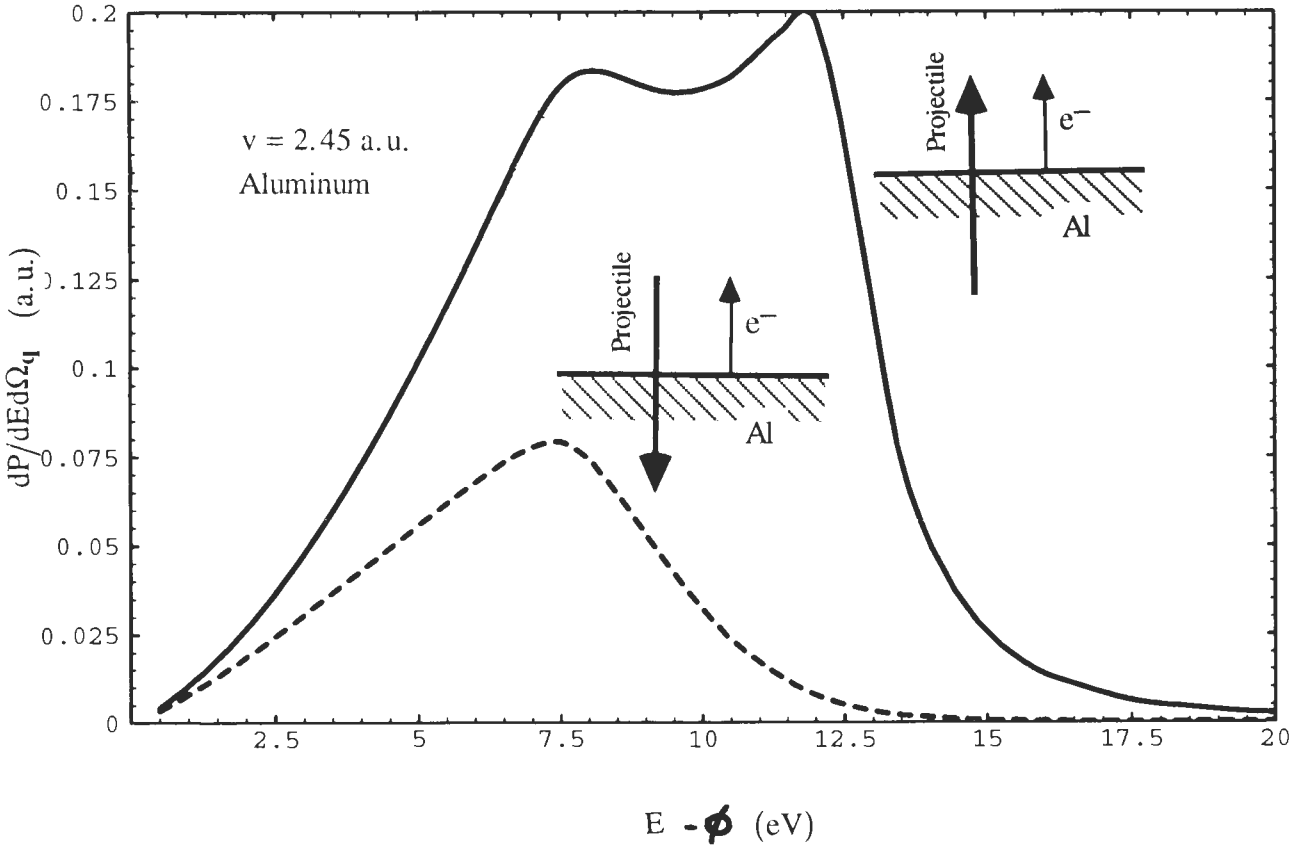

Figure 9. Probability of ejecting electrons along the normal to an aluminum surface, according to eq. (19), as a function of their energy when a 150 keV proton enters or leave the surface (dashed and continuous curves, respectively). The electron energy E-Φ is given relative to the vacuum level. Only electrons that do not suffer any further scattering process since they are excited by the projectile have been considered. The specular-reflection model, together with the Mermin dielectric function [40], has been used to describe the screened potential.

Transmission Geometry

For an arbitrary orientation of the (constant) velocity **v** with respect to the surface, eq. (17) reduces to

$$\frac{dP}{dEd\Omega_q} = \frac{2me^2qq_z}{(2\pi)^4\hbar^4k_z} \cdot \int dk'\theta(E_F-E') \mid \langle k_z \mid \phi(Q,z,\omega) \mid k_z' \rangle \mid^2 . \tag{19}$$

It is important to stress that neither eq. (18) nor eq. (19) incorporate a reliable description of transport, apart from the exponential attenuation of the final wave functions in the solid side (see eq. 16). Thus, no account of electron cascade is given. These equations can be interpreted as describing the electrons emitted without suffering any further scattering once they have been excited.

Figure 9 represents the emission probability for an incoming/outgoing trajectory perpendicular to the surface (dashed/solid curve), when the electron is emitted along the surface normal. It has been calculated from eq. (19), using the same approximations to the surface response as in Figure 8, which incorporates both collective excitations and single-particle excitations. The two peaks appearing in the spectrum for the outgoing trajectory are located at the surface and bulk plasmon energies (relative to the vacuum level) minus the work function, respectively. In the incoming trajectory, the ion interacts during a shorter period of time with the bulk plasmons while it is near the surface. Furthermore, the e-h pair excitations which correspond to the bulk plasma resonance in the response of the medium give rise to the emission of electrons preferentially oriented in the forward direction [65] (Fig. 2a). This may explain why bulk plasmons do not make any contribution to the emission in the incoming trajectory, if one neglects the electron cascade within the present approximation to the surface response. It must be stressed that the dominant true secondary electron peak has to be added to the features presented in Figure 9 in order to compare with experimentally observed spectra; then, these features appear as

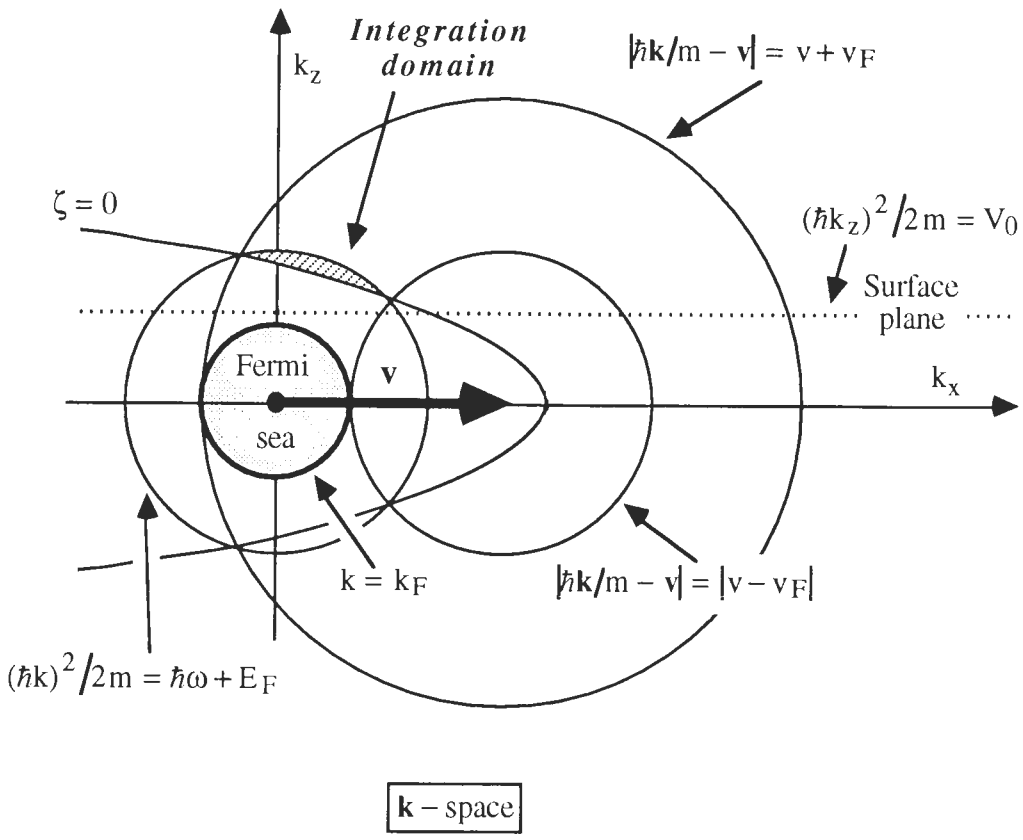

Figure 10. Region of non-vanishing values of ξ in eq. (20). $\xi = 1$ inside the dashed region. The plane of representation of the figure is perpendicular to the k_y axis. All curves have cylindrical symmetry with respect to the k_x axis, except the surface plane, which is perpendicular to the k_z axis.

---

shoulders superimposed to the main secondary electron peak.

The yield of emission associated to the decay of surface plasmons, estimated from Figure 9, is $\Gamma \approx 0.2$ electrons per ion for the outgoing trajectory and $\Gamma \approx 0.06$ for the incoming one. This contribution to the total electron yield tends to enhance the difference of electron emission yield in the forward and backward directions. It represents a small fraction of the experimentally observed yield [28]. Nevertheless, it is enough to create a distinct signature in the derivative of the energy spectra at the energy $\hbar\omega_s$-ϕ [28].

Application to Coincidence Experiments

Next, the theory described in previous sections is applied to recent experimental results on secondary electron emission in coincidence with energy loss events of a primary electron beam [11, 34, 43, 50, 68, 73]. The beam is usually made to cross a thin film (transmission geometry) or directed parallel to one of the faces of a small cube at a distance of a few nm (aloof geometry).

For transmission geometry, the effect of transport (multi-scattering) becomes dominant, since the source of excited electrons extends over all of the depth of the target.

In the aloof geometry, in analogy to the grazing incidence on surfaces discussed previously, the emitted electrons originate in the sub-surface area, and therefore, they are not likely to suffer any further scattering process before they leave the medium. Thus, transport effects are of minor importance and eq. (17) is expected to be a good approximation of the electron emission probability. We will focus on this geometry and neglect transport effects. After some algebra, one finds

$$\frac{d\Gamma}{d\mathbf{k}d\omega} = \xi M_{k\omega}, \tag{20}$$

where

$$M_{k\omega} = \frac{2me^2}{(2\pi\hbar)^3 v} \cdot \int_{-\zeta}^{\zeta} \frac{dk_y'}{k_z'} |\langle k_z | W(Q, z, z_0, \omega) | k_z' \rangle|^2,$$

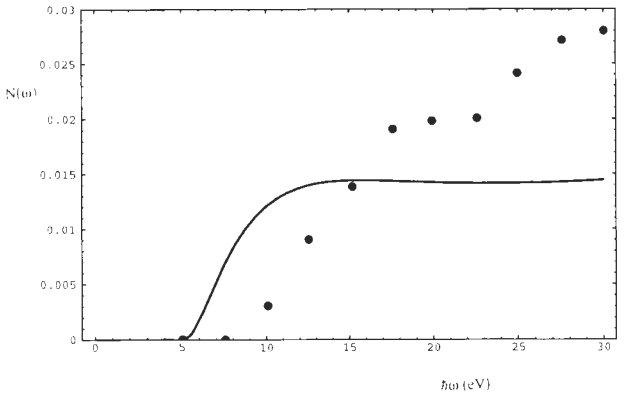

Figure 11. Ratio of a coincidence spectrum to the normal EEL spectrum in the case of an aloof 100 keV e^- beam, for a CVD diamond sample. Experiment [44]: black circles. Theory {eq. (23)}; solid line (electron gas parameters: damping $\hbar\gamma$ = 5 eV, r_s = 1.24).

$\zeta^2 = 2m(E/\hbar^2-\omega/\hbar)-k'_x{}^2$, $k'_x = k_x-\omega/v$, $k'_z{}^2 = \zeta^2-k'_y{}^2$, $E = (\hbar k)^2/2m$ is the electron energy relative to the bottom of the conduction band, and $\xi = 1$ when **k** lies in the dashed region shown in Fig. 10 and vanishes elsewhere. Notice that eq. (18) can also be obtained from eq. (20) by integrating over ω.

In typical coincidence experiments, electrons ejected along different directions with the same energy are simultaneously collected. Therefore, it is convenient to integrate eq. (20) over all possible angles of emission. One obtains

$$\frac{d\Gamma}{dEd\omega} = \frac{2mk}{\hbar^2}\int_{\mu_0}^{\mu_1} d\mu \int_0^{\varphi_1} d\varphi M_{k\omega}, \tag{21}$$

where $\mu = \cos(\mathbf{k},\mathbf{v})$, ϕ is the azimuth angle of **k** in the z-y plane,

$$\varphi_1 = \cos^{-1}\sqrt{V_0/\{E(1-\mu^2)\}},$$

$\mu_0 = \max\{a_-,-b\}$, $\mu_1 = \min\{a_+,b\}$, $a_\pm = (\omega/kv) \pm (1-\hbar\omega/E)^{1/2}$, and $b = (1-V_0/E)^{1/2}$. The energy of the emitted electrons must satisfy the relation $\eta \le E \le \hbar\omega + E_F$, where $\eta = \max\{\hbar\omega, V_0\}$ and V_0 is the height of the surface barrier (Fig. 6).

Since the impact parameter of the primary electron beam z_0 is usually quite large, it is useful to derive the asymptotic behavior of eq. (21) in the $z_0 \to \infty$ limit. After some algebra, one finds, using the solutions of the Schrödinger equation for a step potential of height V_0 as electron wave functions,

$$\frac{d\Gamma}{dEd\omega} = \frac{32(meZ_1)^2}{\pi^3\hbar^5 v^2} K_1\left[\frac{2\omega z_0}{v}\right] \cdot \frac{\omega}{|1+\varepsilon(\omega)|^2} G(E,\omega), \tag{22}$$

where

$$G(E,\omega) = e^2\int_0^{\sqrt{1-\eta/E}} d\mu \cdot \int_0^{\varphi_2} d\varphi \frac{kk_z}{k'_z q_z}|\Sigma_1+\varepsilon(\omega)\Sigma_0|^2,$$

$$\Sigma_0 = \frac{k'_z}{k'_z+ip}\left[\frac{1}{(p+iq_z)^2} - \frac{1}{(p-iq_z)^2}\left(\frac{k_z-q_z}{k_z+q_z}\right)\right],$$

$$\Sigma_1 = \frac{q_z}{k_z+q_z}\left[\frac{1}{(k_z-k'_z)^2} + \frac{1}{(k_z+k'_z)^2}\left(\frac{k'_z-ip}{k'_z+ip}\right)\right],$$

$$\varphi_2 = \cos^{-1}\sqrt{\frac{\eta/E}{1-\mu^2}}, \quad q_z = \sqrt{k_z^2-2mV_0/\hbar^2},$$

$$p = \sqrt{2mV_0/\hbar^2-k'^2_z},$$

$$k_z = k\sqrt{1-\mu^2}\cos\varphi,$$

$$k'_z = \sqrt{k_z^2-2m\omega/\hbar^2},$$

$\epsilon(\omega)$ is the local dielectric function of the bulk material, and K_1 is the modified Bessel function of first order. In obtaining eq. (22), we have made the assumption that $v >> \omega k_F$. Since z_0 is large, the velocity of the primary electrons must also be large so that the argument of the Bessel function in the above equations becomes small in order to guarantee non-negligible contributions to the secondary electron emission. Electron beam energies of the order of 100 keV, typical in STEM, ensure that this condition is fulfilled.

An interesting quantity is provided by the ratio N of $d\Gamma^{coin}/d\omega$ {obtained from eq. (22) by integrating over E} to the differential probability of electron energy loss [12], $d\Gamma^{eels}/d\omega$, given by eq. (14). One finds

$$N = \frac{d\Gamma^{coin}/d\omega}{d\Gamma^{eels}/d\omega} = \frac{8m\omega\theta(\omega-\phi)}{\pi^2\hbar^2 v\,Im\{\varepsilon(\omega)\}} \cdot \frac{K_1(2\omega z_0/v)}{K_0(2\omega z_0/v)} \int_{\eta}^{E_F+\hbar\omega} dE\; G(E,\omega)\,. \tag{23}$$

N represents the probability that an excitation of energy $\hbar\omega$ gives rise to the emission of a secondary electron. In Figure 11, eq. (23) is contrasted to experimental data for the emission of electrons coming from chemical vapor deposited (CVD) diamond in an aloof geometry, taken from reference [44]. A Drude dielectric function has been employed. Despite the simplicity of the model, free of adjustable parameters, the right order of magnitude of N is obtained at the energy corresponding to the surface plasmon, where the Drude model is expected to work best. At energies above the surface plasmon, the experiment shows a linear increase with energy, whereas this theory predicts a constant value for N. This discrepancy may be due to electron multi-scattering, not contained within the present theory. Obviously, the effect of multi-scattering increases with the energy transferred to the medium.

Distribution of Energy Deposited in Electrons and Holes

When an e-h pair is created, the energy deposited in the medium can be divided into (i) the energy of the electron relative to the Fermi level and (ii) the energy difference from the Fermi level to the hole. Both of these terms can be converted into further e-h pairs or other kind of excitations. If one is interested in finding out the way the energy transfer is distributed along the spatial extension of the solid, one has to consider the transport of energy associated with both electrons and holes, each of them involving different mechanisms of propagation [54, 56, 62]. Therefore, it is interesting to know what amount of the energy lost by, e.g., an external particle traversing a solid medium is converted into kinetic energy of electrons {term (i) above} and potential energy of the holes {term (ii)}.

For simplicity, we shall consider a point charge eZ_1 moving with constant velocity v in a homogeneous electron gas. According to the above discussion, the differential stopping power can be written

$$\frac{dS}{d\omega} = \frac{dS^h}{d\omega} + \frac{dS^e}{d\omega} + \frac{dS^{pl}}{d\omega}, \tag{24}$$

where $\hbar\omega$ is the energy loss, $S^{h/e}$ represents the part of the stopping power attributed to holes/electrons, and S^{pl} corresponds to the excitation of plasmons. Now, using the rate of e-h pair creation given in eq. (6), one has

$$\frac{dS^e}{d\omega} = \frac{1}{v}\int d^3k\,d^3k'\,(\hbar\varepsilon_k - E_F)\,\frac{d\Gamma}{d\omega\,d\mathbf{k}\,d\mathbf{k}'}$$

and

$$\frac{dS^h}{d\omega} = \frac{1}{v}\int d^3k\,d^3k'\,(E_F - \hbar\varepsilon_{k'})\,\frac{d\Gamma}{d\omega\,d\mathbf{k}\,d\mathbf{k}'}.$$

These expressions can be further worked out to yield

$$\frac{dS^e}{d\omega} = \frac{2(eZ_1)^2}{\pi v^2} \cdot \int_{q_-}^{q_+}\frac{dq}{q}\left[(\omega - E_F/\hbar)\,Im\left\{\frac{-1}{\varepsilon(q,\omega)}\right\} + \frac{\zeta(q,\omega)}{|\varepsilon(q,\omega)|^2}\right] \tag{25}$$

and

$$\zeta(q,\omega) = \frac{m^2e^2}{\hbar^5 q^3}\cdot(2E_F - \hbar\omega)\,\hbar\omega, \quad \text{for } m\omega/\hbar < q(k_F - \frac{q}{2}); \tag{26}$$

$$= \frac{m^2e^2}{\hbar^5 q^3}\cdot\left[E_F^2 - \frac{1}{64m^2}(2m\omega/q - \hbar q)^4\right], \quad \text{for } q|k_F - q/2| < m\omega/\hbar < q(k_F + q/2);$$

$$= 0, \text{ for rest.}$$

where

The integration limits in eqs. (25) and (26),

$$q_{\pm} = \max\left\{\sqrt{k_F^2 + 2m\omega/\hbar} \pm k_F,\ \omega/v\right\},$$

restrict the possible excitations to the e-h pair region (Fig. 1a).

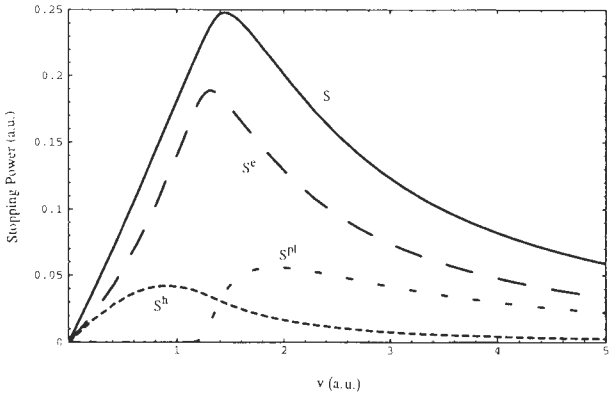

Figure 12. The various contributions to the stopping power of a homogeneous medium to a moving unit charge are shown as a function of the velocity of the charge {eqs. (25 to 27)}. The solid has been described by a gas of independent electrons with density corresponding to that of aluminum. S is the total stopping, S^{pl} is the stopping due to excitation of plasmons, S^{e} is the contribution of the energy transferred to the electrons in e-h pairs, relative to the Fermi level, and S^{h} comes from the energy of the holes relative to the Fermi level.

The plasmon contribution to the stopping power can be extracted from eq. (24) and the total stopping power, related to the dielectric function as

$$\frac{dS}{d\omega} = \frac{2(eZ_1)^2}{\pi v^2}\int_{\omega/v}^{\infty}\frac{dq}{q}\omega Im\left\{\frac{-1}{\varepsilon(q,\omega)}\right\}. \qquad (27)$$

Notice that the sum of e-h pair contributions, that is, eqs. (25) and (26), results in an expression similar to this one with different integration limits ($q_{\pm}$). In eq. (27), the response function is evaluated all over the shaded region of Figure 1a, whereas in the sum of eqs. (25) and (26), it is restricted to the dashed area. Eq. (27) can be obtained by multiplying the loss function by $\hbar\omega/v$ {e.g., taking the $z_0 \to \infty$ limit in eq. (13)}.

Figure 12 compares the magnitude of these contributions to the differential stopping power, calculated from eqs. (25), (26), and (27) integrated over ω. Obviously, the electrons take most of the energy transferred to e-h pairs in the large ω region. The holes take the same energy as the electrons in the $\omega \to 0$ limit. This will also be the case in the $v \to 0$ limit, as shown in Figure 13a. Notice that the plasmon losses appear above the threshold velocity for creation of plasmons, which is such that the line $\omega = qv$ crosses the resonant point C in Figure 1a (v = 1.27 a.u. for Al). For velocities larger than that value, plasmons contribute with losses

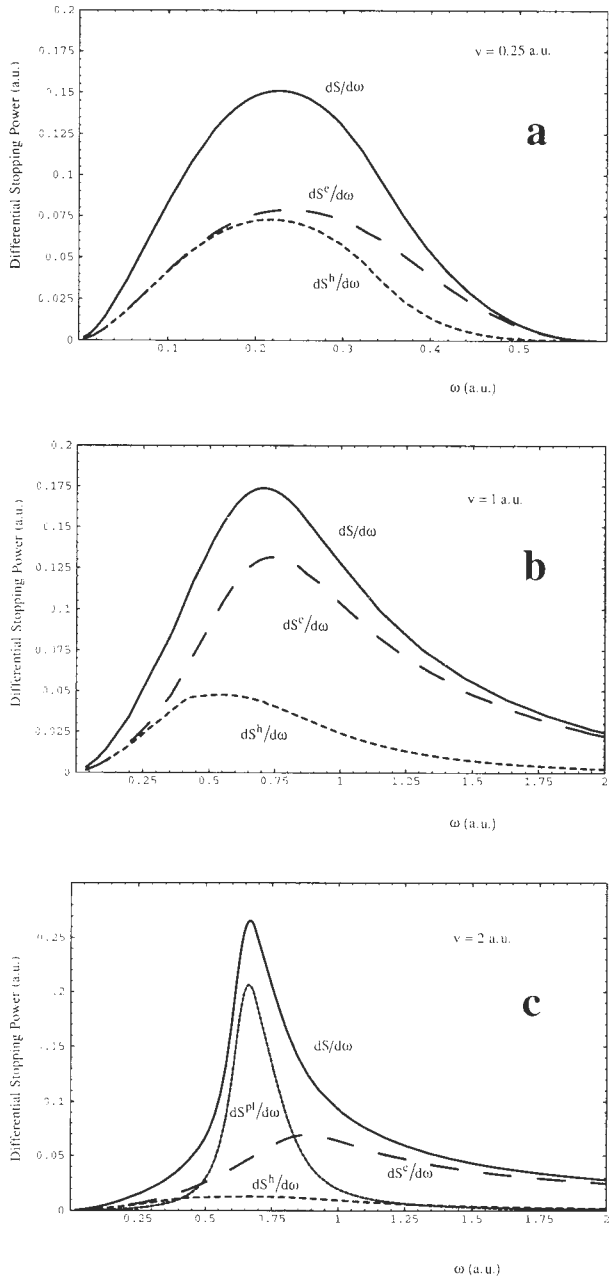

Figure 13. Dependence of the various contributions to the stopping power shown in Figure 12 on the frequency for different particle velocities v = 0.25 (**a**), 1 (**b**) and 2 (**c**) a.u., according to eqs. (25), (26), and (27).

---

peaked at the plasmon frequency (Fig. 13c); they dominate for small ω. Now, since in the large v limit the total energy losses due to the creation of plasmons take approximately the same value as those due to e-h pair creation, this sum rule leads to the conclusion that the differential stopping power has to be dominated by the latter for large ω.

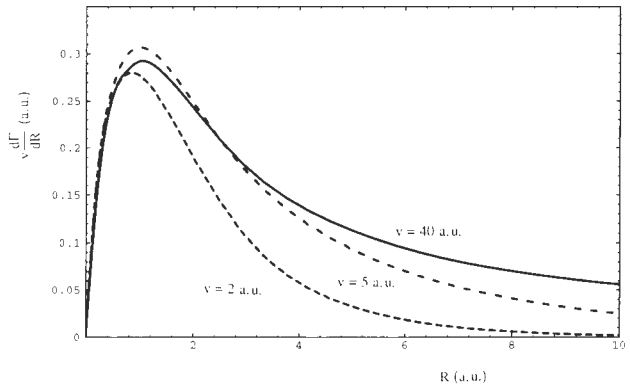

Figure 14. Spatial representation of the excitation probability for a unit charge particle moving inside an electron gas of density equal to that of aluminum with different velocities (2, 5 and 40 a.u.), according to eq. (28). The Mermin dielectric function [40] has been used.

Spatial Representation of the e-h Pair Excitation Probability

The experimental evidence for ion/electron-induced electron emission provides a valuable source of information to analyze the dynamical response of solid media. Nevertheless, transport of excited electrons (and possibly transport of holes as well) makes it difficult to relate experimental observations to the excitation probability itself. Therefore, a quantity that describes the spatial distribution of the latter (i.e., its z-dependence, assuming that the z coordinate runs perpendicular to the surface) would be of some help for that purpose. The electron emission probability would emerge from the spatial convolution of such a quantity with the transport of both electrons and holes from every particular point up to the vacuum. The spatial extension of the track left behind the projectile could be also expressed in these terms.

An impact parameter representation of the mean free path in the homogeneous electron gas has been given recently by Ritchie *et al.* [60, 61] in order to explain the extreme spatial sensitivity of STEM techniques. With our notation, their result can be derived from eq. (1) to obtain the spatial representation of the excitation rate,

$$\frac{d\Gamma}{dR} = \frac{(eZ_1)^2 R}{\pi\hbar}\int_0^\infty dq \int_0^{\pi/2} d\theta\, q^2 \sin 2\theta \times [\sin\theta\, K_0(Rq\sin\theta) J_0(Rq\cos\theta) + \cos\theta\, K_1(Rq\sin\theta) J_1(Rq\cos\theta)] \cdot Im\left\{\frac{-1}{\varepsilon(q, qv\sin\theta)}\right\}, \tag{28}$$

where R is the distance to the trajectory of the external charge, assumed to be moving with constant velocity v. This function has been represented in Figure 14 for a unit charge particle moving inside aluminum with different velocities. In all cases, a peak is found at 1-2 Å from the trajectory.

Similarly, a spatial representation of the excitation probability can be obtained from eq. (1) by expressing the induced current of charge density in terms of the current-density response function η_0, implicitly defined by

$$j^i(\boldsymbol{r},\omega) = \int d^3r' \eta_0(\boldsymbol{r},\boldsymbol{r}',\omega)\,\phi(\boldsymbol{r}',\omega)\,.$$

It reads, in the RPA,

$$\eta_0(\boldsymbol{r},\boldsymbol{r}',\omega) = \frac{-ie^2}{\hbar m}\sum_{k,k'} (f_k - f_{k'}) \times \left(\{\psi_k^*(\boldsymbol{r})[\nabla\psi_{k'}(\boldsymbol{r})] - [\nabla\psi_k^*(\boldsymbol{r})]\psi_{k'}(\boldsymbol{r})\} \cdot \frac{\psi_{k'}^*(\boldsymbol{r}')\psi_k(\boldsymbol{r}')}{\varepsilon_k - \varepsilon_{k'} + \omega + i\gamma}\right), \quad \gamma\to 0^+.$$

Then, the energy loss can be written

$$E = \int_0^\infty d\omega\hbar\omega \int d^3r \sum_{k,k'} \frac{dP_{k,k'}}{dr\,d\omega},$$

where

$$\frac{dP_{k,k'}}{dr\,d\omega} = \frac{e^2}{\pi\hbar m\omega} f_{k'}(1-f_k) \times Im\left\{\left\{\psi_{k'}^*(\boldsymbol{r})[\nabla\psi_k(\boldsymbol{r})] - [\nabla\psi_{k'}^*(\boldsymbol{r})]\psi_k(\boldsymbol{r})\right\} \cdot \frac{\nabla\phi(\boldsymbol{r},\omega)\langle k'|\phi|k\rangle}{\varepsilon_k - \varepsilon_{k'} - \omega - i\gamma} + \left\{\psi_k^*(\boldsymbol{r})[\nabla\psi_{k'}(\boldsymbol{r})] - [\nabla\psi_k^*(\boldsymbol{r})]\psi_{k'}(\boldsymbol{r})\right\} \cdot \frac{\nabla\phi^*(\boldsymbol{r},\omega)\langle k'|\phi|k\rangle}{\varepsilon_k - \varepsilon_{k'} + \omega + i\gamma}\right\} \tag{29}$$

can be interpreted as the spatial representation of the probability of creating a hole in the state k' and an electron in the state k with energy loss $\hbar\omega$.

When eq. (29) is applied to a homogeneous electron gas, the rate of creation of electrons of energy E and holes of energy E' at a distance R from the trajectory, followed by a charge eZ_1 moving with constant velocity v, is found to be

$$\frac{d\Gamma}{dEdE'dR} = \frac{8m^2Z_1^2e^4(E-E')R}{\pi^2\hbar^5v}\int_0^\infty d\omega$$

$$\cdot\ Im\{1/[(E-E')^2-(\hbar\omega+i\gamma)^2]\}$$

$$\times\left[\left[\int_{\omega/v}^\infty J_1(QR)\frac{Qdq}{q\varepsilon(q,\omega)^*}\right]\right.$$

$$\cdot\left[\int_{q_-}^{q_+} J_1(QR)\frac{Qdq}{q^4\varepsilon(q,\omega)}\right]$$

$$+\left(\frac{\omega}{v}\right)^2\left[\int_{\omega/v}^\infty J_0(QR)\frac{dq}{q\varepsilon(q,\omega)^*}\right]$$

$$\left.\cdot\left[\int_{q_-}^{q_+} J_0(QR)\frac{dq}{q^4\varepsilon(q,\omega)}\right]\right] \qquad (30)$$

where J_0 and J_1 are Bessel functions, $Q = (q^2-\omega^2/v^2)^{1/2}$, and

$$q_\pm = \max\{\sqrt{2mE}/\hbar-\sqrt{2mE'}/\hbar,\ \omega/v\}.$$

The spatial representation of electron and hole creation probability, calculated by integration of eq. (30) with respect to hole and electron energies, respectively, is represented in Figures 15 and 16. The latter shows that the holes are mainly produced near the trajectory or near the Fermi level. These functions take negative values for some combinations of R and E (E') as an evidence of their quantal character (they are not really probabilities, but a spatial representation of the probability). The oscillations shown in the figure may also have a quantal nature. Notice that the probability of hole creation receives a certain weight at distances as large as 20 a.u. for v = 10 a.u. (Fig. 16b). Those are holes of low potential energy (E' close to the Fermi level), which are related to the low-energy electron structure observed in Figure 15b at those distances. Thus, this effect represents low-energy e-h pairs, which can be created at distances as large as v/ω, where $\hbar\omega$ is the energy transferred to the e-h pair.

Further research on the spatial distribution of e-h pair creation probability needs to be done in order to apply it to study the transport of electrons created in the bulk and near surfaces.

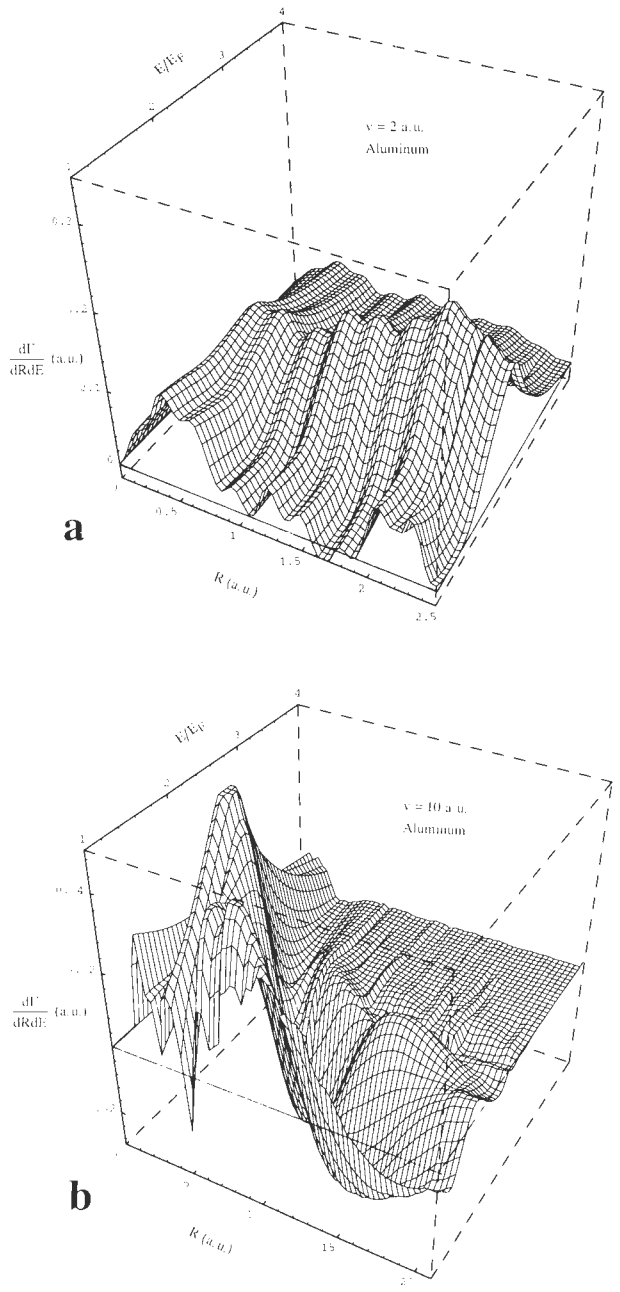

Figure 15. Spatial representation of the rate of creation of electrons shown in Figure 2a, calculated by integration of eq. (30) over E', for v = 2 a.u. and v = 10 a.u.

Conclusions

In this paper, the ion/electron induced electron emission from solids has been analyzed. The concept of surface wake potential, employed here to calculate electron emission probabilities at solid surfaces, has been reviewed. First-order perturbation theory has been used to obtain probabilities of creation of electrons and holes.

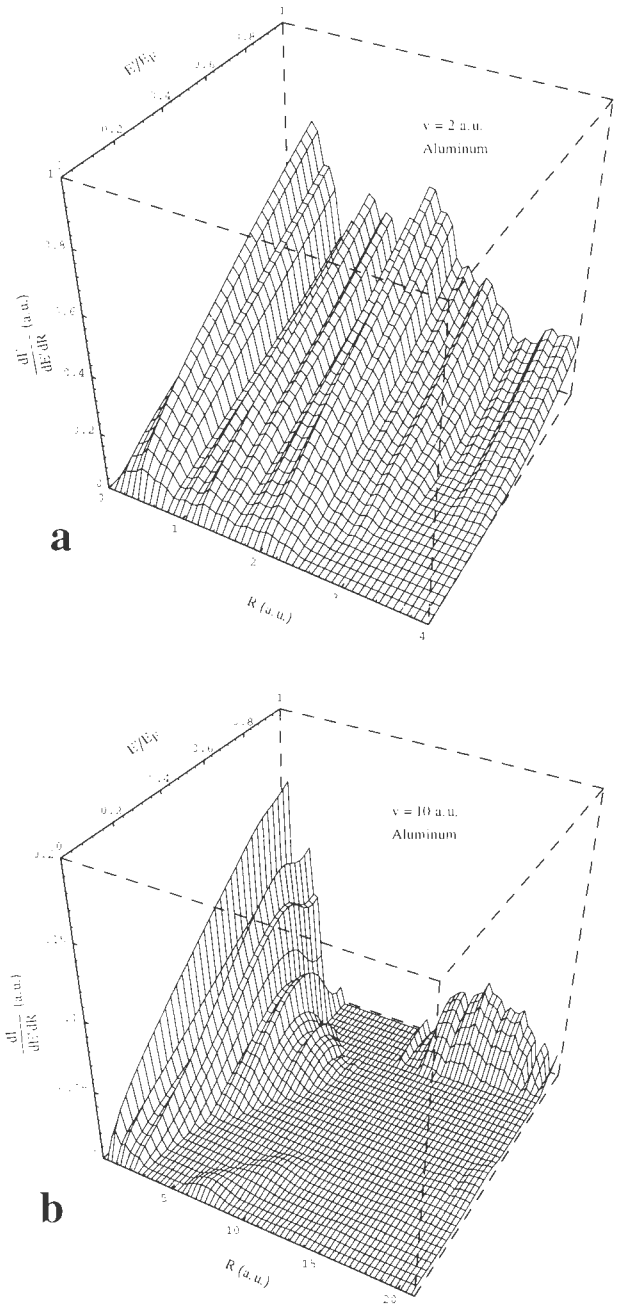

Figure 16. Spatial representation of the rate of creation of holes shown in Figure 2b, calculated by integration of eq. (30) over E, for v = 2 a.u. and v = 10 a.u.

The present theory predicts a significant contribution from surface plasmons to electron emission in grazing particle-surface collisions. The energy spectra of the emitted electrons should present a peak around the energy of the surface plasmon minus the surface work function, in agreement with experimental work by Rau *et al.* [51, 77]. For transmission geometry, bulk and surface plasmons represent a major source of excitation. Reasonable quantitative agreement is found between this theory and recent experiments of coincidence [44] (Fig. 11).

The stopping power of an ion moving inside an electron gas has been decomposed into kinetic energy of excited electrons, potential energy of holes, and creation of plasmons. Electrons and holes share similar amounts of energy at low velocities, whereas the latter take a much smaller portion at large velocities.

Finally, a spatial representation of the probability of creation of electrons and holes by a charge moving inside an electron gas has been derived, finding that the impact parameters, at which the probability take significant values, increase with the velocity of the charge.

Acknowledgements

The author expresses his gratitude to R.H. Ritchie and P.M. Echenique for many stimulating discussions. The help and support by the Departamento de Educación del Gobierno Vasco, the Diputación Foral de Guipúzcoa, the University of the Basque Country, and the European Union under contract ERB CHRXCT 940571 are thankfully acknowledged.

References

[1] Ashley JC, Tung CJ, Ritchie RH (1979) Electron inelastic mean free paths and energy losses in solids. Surf Sci **81**: 409-426.

[2] Baroody EM (1950) A theory of secondary electron emission from metals. Phys Rev **78**: 780-787.

[3] Boersch H, Geiger J, Stickel W (1968) Anregung von Kristallgitterschwingungen durch Elektronenstrahlen (Excitation of crystal lattice oscillations by electron beams). Z Phys **212**: 130-145.

[4] Brice D, Sigmund P (1980) Secondary electron spectra in the free electron gas. Mat Phys Medd Dan Vid Selsk **40**: no. 8, 5-34.

[5] Bruining H (1954) Physics and Applications of Secondary Electron Emission. Pergamon Press, London. p. 137.

[6] Burkhard M, Rothard H, Biedermann C, Kemmler J, Kroneberger K, Koschar P, Heil O, Groeneveld KO (1987) Heavy-ion-induced shock electrons from sputter-cleaned solid surfaces. Phys Rev Lett **58**: 1773-1775.

[7] Chan D, Richmond P (1976) Static and dynamic interactions with spatially dispersive media. J Phys **C9**: 163-168.

[8] Chung MS, Everhart TE (1977) Role of plasmon decay in secondary electron emission in the nearly-free-electron metals. Application to aluminum. Phys Rev

B15: 4699-4715.

[9] Cowley JM (1982) Surface energies and structure of small crystals. Surf Sci **114**: 587-606.

[10] Devooght J, Dehaes JC, Dubus A, Cailler M, Ganachaud JP (1991) Theoretical description of secondary electron emission induced by electron or ion beams impinging on solids. In: Particle Induced Electron Emission I. Höhler G, Niekisch EA (eds.). Springer Tracts in Modern Physics **122**: 67-128.

[11] Drucker J, Schenfein MR (1993) Delocalized secondary-electron generation studied by momentum-resolved coincidence-electron spectroscopy. Phys Rev **B47**: 15973-15975.

[12] Echenique PM, Pendry JB (1975) Absorption profile at surfaces. J Phys **C8**: 2936-2942.

[13] Echenique PM, Ritchie RH, Brandt W (1979) Spatial excitation patterns induced by swift ions in condensed matter. Phys Rev **B20**: 2567-2580.

[14] Echenique PM, Bausells J, Rivacoba A (1987) Energy-loss probability in electron microscopy. Phys Rev **B35**: 1521-1524.

[15] Echenique PM, Flores F, Ritchie RH (1990) Dynamic screening of ions in condensed matter. Solid State Phys **43**: 229-308.

[16] Eguiluz AG (1985) Self-consistent static-density-response function of a metal surface in density-functional theory. Phys Rev **B31**: 3303-3314.

[17] Eriksson HG, Karlsson BR, Wijewardena KAIL (1985) Oscillatory polarization potential induced at a surface by a penetrating charge. Phys Rev **B31**: 843-849.

[18] Ferrel TL, Echenique PM (1985) Generation of surface excitations of dielectric spheres by an external electron beam. Phys Rev Lett **55**: 1526-1529.

[19] Flores F, García-Moliner F (1979) Self-energy of a fast-moving charge near a surface. J Phys **C12**: 907-924.

[20] García de Abajo FJ (1995) The role of surface plasmons in ion-induced kinetic electron emission. Nucl Instr Meth **B98**: 445-449.

[21] García de Abajo FJ, Echenique PM (1992) Wake-potential formation in a thin film Phys Rev **B45**: 8771-8774.

[22] García de Abajo FJ, Echenique PM (1992) Wake potential in the vicinity of a surface. Phys Rev **B46**: 2663-2675.

[23] García de Abajo FJ, Echenique PM (1993) Surface wake in the random-phase approximation. Phys Rev **B48**: 13399-13407.

[24] García de Abajo FJ, Echenique PM (1993) Ion-induced electron emission in grazing ion-surface collisions. Nucl Instr Meth **B79**: 15-20.

[25] Gaspar JA, Eguiluz AG, Mills DL (1995) Theory of ion-stimulated electron emission from simple metals: Explicit calculations. Phys Rev **B51**: 14604-14611.

[26] Glasser ML, Gumbs G (1987) Screened potential for planar charged sheets within a semi-infinite Landau-quantized plasma. Phys Rev **B35**: 7490-7495.

[27] Gumbs G, Glasser ML (1988) Wake potential of a swift ion near a metal surface. Phys Rev **B37**: 1391-1394.

[28] Hasselkamp D (1991) Kinetic electron emission from solid surfaces under ion bombardment. In: Particle Induced Electron Emission II. Höhler G, Niekisch EA (eds.). Springer Tracts in Modern Physics **123**: 1-95.

[29] Hegmann A, Zimny R, Ortjohann HW, Winter H, Miskovic ZL (1994) Angle-resolved emission of low-energy electrons in grazing collisions of protons with an Al(111)-surface. Europhys Lett **26**: 383-388.

[30] Heinrichs J (1973) Response of metal surfaces to static and moving point charges and to polarizable charge distributions. Phys Rev **B8**: 1346-1364.

[31] Horing NJM, Tso HC, Gumbs G (1987) Fast-particle energy loss in the vicinity of a two-dimensional plasma. Phys Rev **B36**: 1588-1594.

[32] Howie A, Milne RH (1985) Excitations at interfaces and small particles. Ultramicroscopy **18**: 427-434.

[33] Inglesfield JE, Wikborg E (1974) Surface plasmons in free-electron metals. Solid State Commun **14**: 661-664.

[34] Kruit P (1993) Nanometer resolution analysis of surfaces. Surf Sci **287/288**: 1067-1069.

[35] Libenson BN, Rumyantsev VV (1984) Energy loss by a fast charged particle moving parallel to a surface. Sov Phys JETP **59**: 999-1005.

[36] Lindhard J (1954) On the properties of a gas of charged particles. Kgl Dans Vidensk Selsk Mat Fys Medd **28**: no. 8, 1-57.

[37] Lucas AA, Sunjic M (1972) Fast-electron spectroscopy of surface excitations. Phys Rev Lett **26**: 229-232.

[38] Lundqvist BI (1967) Single-particle spectrum of the degenerate electron gas II. Phys Kondens Mater **6**: 206-217.

[39] Marks LD (1982) Observation of the image force for fast electrons near an MgO surface. Solid State Commun **43**: 727-729.

[40] Mermin ND (1970) Lindhard dielectric function in the relaxation-time approximation. Phys Rev **B1**: 2362-2363.

[41] Messiah A (1964) Quantum Mechanics. Wiley, New York. pp. 328-329.

[42] Mills DL (1993) Theory of electron emission stimulated by charged particle reflection from simple metals; glancing incidence. Surf Sci **294**: 161-183.

[43] Müllejans H (1992) Secondary electron emis-

sion in coincidence with primary energy losses. Doctoral Thesis. University of Cambridge, U.K. pp. 58-59.

[44] Müllejans H, Bleloch AL, Howie A, Tomita M (1993) Secondary electron coincidence detection and time-of-flight spectroscopy. Ultramicroscopy **52**: 360-368.

[45] Neufeld J, Ritchie RH (1955) Passage of charged particles through plasma. Phys Rev **98**: 1632-1642.

[46] Neufeld J, Ritchie RH (1955) Density effect in ionization energy loss of charged particles. Phys Rev **99**: 1125-1128.

[47] Newns DM (1970) Dielectric response of a semi-infinite degenerate electron gas. Phys Rev **B1**: 3304-3322.

[48] Núñez R, Echenique PM, Ritchie RH (1980) The energy loss of energetic ions moving near a solid surface. J Phys **C13**: 4229-4246.

[49] Penn DR (1987) Electron mean-free-path calculations using a model dielectric function. Phys Rev **B35**: 482-486.

[50] Pijper FJ, Kruit P (1991) Detection of energy-selected secondary electrons in coincidence with energy-loss events in thin carbon foils. Phys Rev **B44**: 9192-9200.

[51] Rau C, Zheng NJ (1993) Grazing-angle ion-induced electron excitation at metal surfaces. J Phys: Condens Matter **5**: A249-A252.

[52] Ritchie RH (1957) Plasma losses by fast electrons in thin films. Phys Rev **106**: 874-881.

[53] Ritchie RH (1959) Interaction of charged particles with a degenerate Fermi-Dirac electron gas. Phys Rev **114**: 644-654.

[54] Ritchie RH (1966) Coupled electron-hole cascade in a free electron gas. J Appl Phys **37**: 2276-2278.

[55] Ritchie RH (1981) Quantal aspects of the spatial resolution of energy-loss measurements in electron microscopy. Phil Mag **A44**: 931-942.

[56] Ritchie RH, Ashley JC (1965) The interaction of hot electrons with a free electron gas. J Phys Chem Solids **26**: 1689-1694.

[57] Ritchie RH, Howie A (1988) Inelastic scattering probabilities in scanning transmission electron microscopy. Phil Mag **A58**: 753-767.

[58] Ritchie RH, Marusak AL (1966) The surface plasmon dispersion relation for an electron gas. Surf Sci **4**: 234-240.

[59] Ritchie RH, Garber FW, Nakai MY, Birkhoff RD (1969) Low energy electron mean free paths in solids. Adv Rad Biol **3**: 1-28.

[60] Ritchie RH, Hamm RN, Turner JE, Wright HA, Ashley JC, Basbas GJ (1989) Physical aspects of charged particle track structure. Nucl Tracks Radiat Meas **16**: 141-155.

[61] Ritchie RH, Howie A, Echenique PM, Basbas GJ, Ferrell TL, Ashley JC (1990) Plasmons in scanning transmission electron microscopy electron spectra. Scanning Microsc Suppl **4**: 45-56.

[62] Ritchie RH, Hamm RN, Ashley JC, Echenique PM (1991) Electron spectra in solids. In: Interaction of Charged Particles with Solids and Surfaces. Gras-Martí A, Urbassek HM, Arista NR, Flores F (eds.). Plenum Press, New York. pp. 197-225.

[63] Rivacoba A, Echenique PM (1990) Surface corrections to bulk energy losses in scanning transmission electron microscopy of spheres. Scanning Microsc **4**: 73-78.

[64] Romanov YuA, Aleshkin VYa (1981) Interaction of charges moving near the surface of a solid. Sov Phys Solid State **23**: 47-49.

[65] Rösler M, Brauer W (1991) Theory of electron emission from nearly-free-electron metals by proton and electron bombardment. In: Particle Induced Electron Emission I. Höhler G, Niekisch EA (eds.). Springer Tracts in Modern Physics **122**: 1-65.

[66] Rothard H, Kroneberger K, Burkhard M, Biedermann C, Kemmler J, Heil O, Groeneveld KO (1989) Refraction of directed shock electrons at planar solid surfaces. J de Physique **50**(C2): 105-110.

[67] Rutherford E (1905). Charge carried by the α and β rays of radium. Phil Mag **10**: 193-208.

[68] Scheinfein MR, Drucker J, Weiss JK (1993) Secondary-electron production pathways determined by coincidence electron spectroscopy. Phys Rev **B47**: 4068-4071.

[69] Schou J (1988) Secondary electron emission from solids by electron and proton bombardment. Scanning Microsc **2**: 607-632.

[70] Sternglass EJ (1957) Theory of secondary electron emission by high-speed ions. Phys Rev **108**: 1-12.

[71] Suzuki K, Kitagawa M, Ohtsuki YH (1977) Theory of surf-riding electrons on the wake potential of ion beams in a metal. Phys Stat Sol **B82**: 643-650.

[72] Thomson JJ (1904) On the positive electrification of α rays, and the emission of slowly moving cathode rays by radio-active substances. Proc. of the Cambridge Philosophical Soc. **13**: 49-54.

[73] Voreades D (1976) Secondary electron emission from thin carbon films. Surf Sci **60**: 325-348.

[74] Wilems RE (1968) Nonlinear interactions in quantum plasmas. Doctoral Thesis. University of Tennessee. Also published as an Oak Ridge Natl Lab Report ORNL-TM-2101 authored by Wilems RE, Ritchie RH.

[75] Wolff PA (1954) Theory of secondary electron cascade in metals. Phys Rev **95**: 56-66.

[76] Zabala N, Echenique PM (1990) Energy loss of fast electrons moving near plane boundaries with

dispersive media. Ultramicroscopy **32**: 327-335.

[77] Zheng NJ, Rau C (1993) Excitation of quasiparticles during grazing-angle ion reflection at Al surfaces. J Vac Sci Technol **A11**: 2095-2098.

Discussion with Reviewers

H. Müllejans: In the last sentence of the paper, referring to Figures 15 and 16, you say that negative values are an evidence for the quantal character. Could you please clarify this point further? Do negative intensities indicate annihilation rather than creation of electrons and holes?

Author: The calculations leading to those figures assume that the medium is initially prepared in its ground state. Therefore, electrons and holes cannot be annihilated within the framework of first-order perturbation theory used here. The data displayed in the figure constitute a spatial representation of electron and hole creation probability: they give an idea of how much a given impact parameter R contributes to the probability. Therefore, they are not probabilities, and can take negative values in some places.

H. Müllejans: In Figure 9, you show the probability of electron ejection for an incident proton. If this is calculated for an incident electron, are the differences as pronounced? Do the calculations for incident electrons compare to experiments?

Author: The present theory does not discriminate between incident electrons and protons. The incident projectile is considered to have infinite mass. An electron traveling with the same velocity as the proton of Figure 9 would have 81 eV, for which that approximation is questionable. On the other hand, both for incident protons and for incident electrons, the transport of the excited electrons that suffer scattering processes before they leave the surface, as well as cascade electrons, must be added to the spectra depicted in Figure 9 in order to properly compare to experiments.

H. Müllejans: It would be interesting to see the results for the differential stopping power (Fig. 13) for incident electrons of 100 keV primary energy.

Author: The results for 100 keV primary electrons look very similar to those shown in Figure 13c, except that $dS^h/d\omega$ is almost negligible and $dS^e/d\omega$ is much smaller than the plasmon losses for $\omega < 1$ a.u. $dS^e/d\omega$ dominates for large ω. That is, plasmons dominate for small ω, whereas the target electrons behave like free electrons at rest for large energy transfers $\hbar\omega$.

H. Müllejans: How does the spatial representation of e-h pair creation relate to the spatial resolution observed in electron microscopes for secondary electron and plasmon loss imaging?

Author: Following the argument given by Ritchie *et al.* [61], from Figure 14, one concludes that the impact parameters of relevance are below 1 nm, keeping in agreement with Figs. 15 and 16 and with the experimentally observed spatial resolution.

R.H. Ritchie: Results found for the spatial dependence of electron-hole pair generation are shown in the last two graphs, but are a bit difficult to read. Qualitatively, one would expect that the differential probability of e-h creation should decrease quite a bit faster with increasing distance from the ion track than does the probability of bulk plasmon creation. Is this confirmed in the detailed results? Can one characterize the e-folding distance in space for a representative group of electrons or holes?

Author: The answer to the first question is yes. Figure 14 contains both plasmon excitations and e-h pairs, whereas Figures 15 and 16 contain only the latter. The integral over the whole hole energy range in Figure 16a yields a curve which lies below and decreases faster with R than the one corresponding to $v = 2$ a.u. in Figure 14. Concerning the e-folding distance, v/ω, one can observe in Figure 15b that the maximum impact parameter below which $d\Gamma$ takes significant values decreases with increasing energy E. Also, Figure 16b shows that the holes with the largest potential energies (minimum E') pile up near $R = 0$.

R.H. Ritchie: Figure 5b nicely illustrates the operation of the boundary (or begrenzung) effect in surface and bulk plasmon excitation. There is a maximum in the probability of surface plasmon excitation as a function of the position of the ion relative to the surface, but it occurs in this figure not exactly at the surface. Why is this?

Author: When the ion travels in the vacuum side or on the surface, the position of the centroid of induced charge is placed below the surface in the specular-reflection model if one uses a bulk dielectric function with a positive plasmon dispersion relation (Fig. 5). Therefore, since the strength of the surface plasmon is connected to the convolution of the bare potential with the induced charge, the maximum in the losses due to the creation of surface plasmons do not have to be placed right at the surface, but displaced towards the solid. How much it is displaced depends on the actual value of the damping and on the magnitude of the dispersion.

M. Rösler: In reference [29], two different features of the electron emission (the proton impact energies are

below 30 keV) were observed. At low energies, a structure appears, which is located (in energy) in the same region as the calculated feature shown in Figure 8 (which shows an enhanced emission in forward direction and a small shift of the energetic position). The observed structure is independent of the angle of emission and nearly independent of the impact energy [29]. The second feature appears in the spectra of [29] at distinct higher energies (in this case, there is a shift to higher energies with increasing impact energy). These high-energy electrons are emitted preferentially in the forward direction. I believe that it is not possible to compare this emission feature with the calculated structure shown in Figure 8. Can you give a comment?

Author: The high-energy peak in reference [29] seems to behave with velocity like a binary peak. The low-energy peak intensity shows a $\cos(\theta)$ angular dependence similar to Figure 8. Unlike what happens in Figure 8, it cannot be ascribed to the decay of surface plasmons directly created by the projectile, since this travels with velocities under the threshold needed to create plasmons.

H. Rothard: Consider heavy ions or clusters instead of protons and electrons. Can the much stronger perturbation and ionization density with this heavy projectiles be treated within linear theory? How can charge exchange and excited projectile states be included?

Author: That depends on the velocity of the projectiles. For relatively low velocities (smaller than the projectile charge), one should consider using non-linear approaches. Charge exchange and excited projectile states are commonly treated within first-order perturbation theory in cases like Auger charge transfer (see reference [15] for details).

H. Rothard: Brice and Sigmund [4] calculated "secondary electron spectra from dielectric theory," and found a resonance in angular distributions at emission angles $\theta = \cos^{-1}(v_s/v_p)$ (Mach relation with a shock wave group velocity v_s and projectile velocity v_p) which were interpreted as emission of low energy shock electrons [additional reference 78]. What are the similarities and differences between the calculations of Brice and Sigmund [4] and the formalism that you apply? In Figure 8, you show energy spectra for perpendicular electron emission. It should be possible to calculate double differential electron energy and angular distributions within your theory. Can you say something about the angular dependence of the peaks seen in Figure 8? Is there a resonance of the type mentioned above?

Author: The dielectric theory used here for the homogeneous electron gas fully coincides with that first given by Ritchie [53] and also with the calculations performed by Brice and Sigmund [4]. The derivation given here is somewhat different, allowing us to study electron excitation at surfaces and derive a spatial representation of the e-h excitation probability. The resonance in the distribution in angle and energy pointed out in reference [4] is the same as that illustrated in Figure 2a. In the present work, the distribution of holes is given as well. In Figure 8, the emitted electron is considered to form an angle θ with the surface normal, so that the angular dependence of the emission is shown there. In this case, there is not a resonance of the kind commented above (see discussion on point C in Fig. 1). The electrons are preferentially emitted in the forward direction due to momentum conservation.

Additional Reference

[78] Schäfer W, Stöcker H, Müller G, Greiner W (1980) Mach shock electron distributions from solids. Z Phys **B36**: 319-322.